Article

Immunity

Interleukin-6 produced by enteric neurons regulates the number and phenotype of microbe-responsive regulatory T cells in the gut

Graphical Abstract

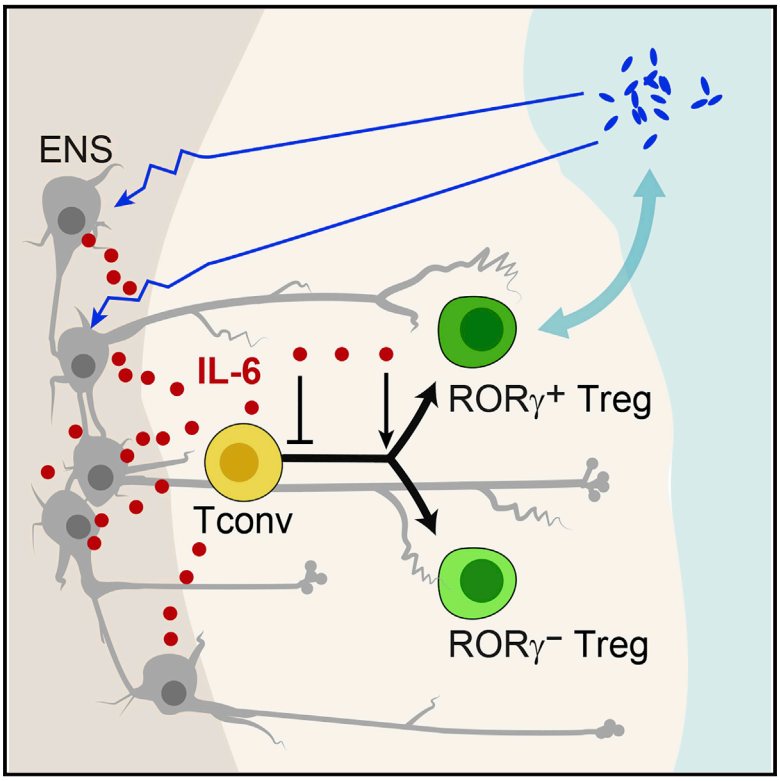

Authors

Yiqing Yan, Deepshika Ramanan, Milena Rozenberg, ..., Meenakshi Rao, Diane Mathis, Christophe Benoist

Correspondence

cbdm@hms.harvard.edu

In brief

Regulatory T (Treg) cells lie in proximity to nerve fibers in the colon lamina propria. Yan et al. reveal a regulatory circuit wherein microbial signals condition neuronal density and activation, which in turn, via neuron-produced IL-6, tunes Treg cell generation, which has implications for intestinal tolerance.

Highlights

- Treg cells in the colon lamina propria reside close to neuron projections
- Neurons modulate the differentiation and phenotype of iTreg cells in culture via IL-6
- Neuron-specific ablation of *Il6* increases the number of RORγ$^+$ Treg cells *in vivo*
- Microbial colonization affects a subset of neurons in the enteric nervous system

Yan et al., 2021, Immunity *54*, 499–513
March 9, 2021
https://doi.org/10.1016/j.immuni.2021.02.002

CellPress

Immunity

CellPress

Article

Interleukin-6 produced by enteric neurons regulates the number and phenotype of microbe-responsive regulatory T cells in the gut

Yiqing Yan,[1] Deepshika Ramanan,[1] Milena Rozenberg,[2] Kelly McGovern,[3] Daniella Rastelli,[3] Brinda Vijaykumar,[1] Omar Yaghi,[1] Tiphaine Voisin,[1] Munir Mosaheb,[1] Isaac Chiu,[1] Shalev Itzkovitz,[2] Meenakshi Rao,[3] Diane Mathis,[1] and Christophe Benoist[1,4,*]

[1]Department of Immunology, Harvard Medical School, Boston MA 02115, USA
[2]Department of Molecular Cell Biology, Weizmann Institute of Science, Rehovot 7610001, Israel
[3]Department of Pediatrics, Boston Children's Hospital, Boston, MA 02115, USA
[4]Lead contact
*Correspondence: cbdm@hms.harvard.edu
https://doi.org/10.1016/j.immuni.2021.02.002

SUMMARY

The immune and enteric nervous (ENS) systems monitor the frontier with commensal and pathogenic microbes in the colon. We investigated whether FoxP3$^+$ regulatory T (Treg) cells functionally interact with the ENS. Indeed, microbe-responsive RORγ^+ and Helios$^+$ subsets localized in close apposition to nitrergic and peptidergic nerve fibers in the colon lamina propria (LP). Enteric neurons inhibited *in vitro* Treg (iTreg) differentiation in a cell-contact-independent manner. A screen of neuron-secreted factors revealed a role for interleukin-6 (IL-6) in modulating iTreg formation and their RORγ^+ proportion. Colonization of germfree mice with commensals, especially RORγ^+ Treg inducers, broadly diminished colon neuronal density. Closing the triangle, conditional ablation of IL-6 in neurons increased total Treg cells but decreased the RORγ^+ subset, as did depletion of two ENS neurotransmitters. Our findings suggest a regulatory circuit wherein microbial signals condition neuronal density and activation, thus tuning Treg cell generation and immunological tolerance in the gut.

INTRODUCTION

The mammalian intestinal tract is one of the main ports of exchange between the organism and the outside world. It is not solely a barrier but must maintain an intimate dialog with nutritional sources and with the microbial symbionts that assist in food processing. This frontier is closely monitored by both the immune and nervous systems, which together discriminate between nutritionally valuable versus harmful chemical entities and symbiotic versus pathogenic microbes. The enteric nervous system (ENS) is the largest neural organ outside the brain, can function largely autonomously, responding to and adapting to local challenges (Furness et al., 2014; Kulkarni et al., 2018; Zeisel et al., 2018). The ENS includes a full repertoire of sensory neurons, interneurons, and motor neurons that collectively detect luminal contents, drive secretory function, and control intestinal motility (Furness et al., 2013; Yang and Chiu, 2017). Enteric neurons are organized within two sets of ganglionated plexuses, the submucosal plexus, which contains many neurons projecting to the mucosa, and the myenteric plexus located within the muscularis externa. The gut is a large lymphoid organ as well, with an architecture, cell composition, and traffic patterns distinct from those of all other organismal locations; it also closely monitors luminal content through arrays of innate and adaptive receptors.

Perhaps predictably, there is crosstalk between the two systems (Margolis et al., 2016; Veiga-Fernandes and Mucida, 2016; Yoo and Mazmanian, 2017; Huh and Veiga-Fernandes, 2020). Macrophages influence the regulation of gut motility, are necessary for ENS homeostasis, and are reciprocally influenced by β2-adrenergic agonists or colony stimulating factor 1 (CSF1) released by neurons, all of which generally promote homeostasis and rapid tissue-protective responses (Muller et al., 2014; Gabanyi et al., 2016; De Schepper et al., 2018). Interactions between the ENS and innate like lymphocytes (ILCs) have also been described: the neuropeptides neuromedin U (NMU) and calcitonin gene-related peptide (CGRP) regulate ILC2 maturation and activation, whereas neurotrophic factors of the glial cell-derived neurotrophic factor (GNDF) family support interleukin-22 (IL-22)-producing ILC3s (Klose et al., 2017; Cardoso et al., 2017; Wallrapp et al., 2019; de Jong et al., 2015). Mucosal nerves occur adjacent to ILC2s, and glial cell projections are in close contact with ILC3s (Ibiza et al., 2016; Cardoso et al., 2017).

Regulatory T (Treg) cells that express the transcription factor Foxp3 Treg cells are a subset of CD4$^+$ T cells that control innate and adaptive immune responses (Josefowicz et al., 2012) and

also have broader functions in maintaining tissue homeostasis in non-immunologic settings (Panduro et al., 2016). Treg cells are also key players in host-pathogen immunity (Schiering et al., 2014), in particular in the gut where their numbers and phenotypes are tuned by commensal microbes (Lathrop et al., 2011; Nutsch et al., 2016; Atarashi et al., 2011; Sefik et al., 2015; Ohnmacht et al., 2015; Al Nabhani et al., 2019; Pratama et al., 2020). Two distinct subpopulations of intestinal Foxp3$^+$ Treg cells have been distinguished. The first expresses the nuclear hormone receptor RORγ and the transcription factor (TF) c-Maf (Ohnmacht et al., 2015; Sefik et al., 2015; Yang et al., 2016; Yissachar et al., 2017; Xu et al., 2018; Neumann et al., 2019; Wheaton et al., 2017). They predominate in the colon and are induced by commensal microbes, with highly varying efficacy between microbial species (Sefik et al., 2015), and through several potential mechanisms (Verma et al., 2018; Yissachar et al., 2017; Hang et al., 2019; Song et al., 2020). The second subset expresses Helios and Gata3, predominates in the small intestine (Wohlfert et al., 2011; Schiering et al., 2014; Sefik et al., 2015; Ohnmacht et al., 2015), and is less dependent on the microbiota but might respond more to tissue stress (Peine et al., 2016; Molofsky et al., 2015) mediated via the alarmin interleukin IL-33 (Schiering et al., 2014; He et al., 2017). RORγ$^+$ and Helios$^+$ Treg cells have non-redundant functions, given that genetic inactivation of RORγ$^+$ Treg cells influences disease severity in colitis models, food allergy, and colorectal tumors (Sefik et al., 2015; Ohnmacht et al., 2015; Neumann et al., 2019; Xu et al., 2018; Al Nabhani et al., 2019; Neumann et al., 2019; Ye et al., 2017).

Beyond the canonical role of Treg cells in controlling neurological autoimmunity or inflammation, evidence for peripheral neuro-immune interactions involving Treg cells is somewhat limited. Interaction between CNS neurons and T cells promotes the conversion of potentially encephalitogenic T cells to Treg phenotypes (Liu et al., 2006). Treg cells in the muscle are associated with nerve fibers and muscle spindles, and nerve-associated stromal cells enhance Treg function via IL-33 to promote muscle repair (Kuswanto et al., 2016). In a recent report, perturbations of vagal sensory afferents reduced the proportions of colonic Treg cells via intestinal antigen-presenting cells (Teratani et al., 2020). While exploring the mechanism of RORγ$^+$ Treg cell induction by gut commensals in germ-free (GF) mice, we noted an intriguing relation between the ability of bacterial species to induce these Treg cells and their ability to trigger neuronal populations, manifest as changes in gene expression in the ENS or as induction of action potential firing of dorsal root ganglia (DRG) sensory neurons (Yissachar et al., 2017). In addition, colonic RORγ$^+$ Treg cell frequencies were altered in mice fed a capsaicin-rich diet or lacking tachykinin precursor 1 (TAC1), the precursor protein for the neuropeptide substance P and neurokinin A.

These relationships suggest a direct crosstalk between the ENS and colonic Treg cells. Here, we examined the functional interactions between ENS and Treg cells, as well as the effect of microbiota given its role in driving Treg cell differentiation in the gut. Treg cells located in very close vicinity to neuronal fibers in the lamina propria (LP). *In vitro*, enteric neurons modulated iTreg differentiation, reducing overall FoxP3 induction but promoting RORγ$^+$ Treg cell proportions, an action that genomic and genetic explorations established as linked to IL-6 produced by neurons. *In vivo*, microbial colonization perturbed the ENS, reducing its ability to express IL-6. Neuron-specific ablation of IL-6 correspondingly affected Treg cell numbers and phenotypes. These data suggest a three-way interaction that controls tolerance at the microbial interface.

RESULTS

Colonic Treg cells localize closely to neurons

Our earlier results (Yissachar et al., 2017) evoked a crosstalk between neurons and Treg cells in the gut wall. To determine the possibility of a direct interaction, we performed immunofluorescence imaging on segments of mouse colon, asking whether Treg cells were located near neuronal bodies in enteric ganglia or their projections in the (LP) (Figure 1A). On transverse sections of the colon, counterstained with neuronal (anti-βIII-Tubulin and Tuj1) and epithelial (EpCam1) markers, FoxP3$^+$ Treg cells identified via the *Foxp3-gfp* reporter were seen at different levels of the LP (Figure 1B), but were rarely if ever detected in the myenteric plexus or muscularis externa. Whole-mount imaging of optically cleared tissue showed that Treg cells were located very close to, and organized along, the "honeycomb" of neuronal fibers projecting in the LP around colonic epithelial glands (Figures 1C and S1A). For comparison, staining for F4/80$^+$ macrophages showed them more continuously aligned with the nerve fibers, as reported (Gabanyi et al., 2016), and less scattered than Treg cells (Figure S1A). Unlike macrophages, Treg cells were rare or absent in the myenteric plexus, indicating that they do not contact the cell bodies of myenteric neurons (Figures 1D and S1B). To define the category of nerve fibers contacted by Treg cells, we counterstained thin section of colonic LP for CGRP (a product of *Calca* or *Calcb* genes in afferent neurons of both the myenteric plexus and the dorsal root ganglion [DRG]) and nitric oxide synthase (NOS1) (which predominantly identifies nitrergic inhibitory motor neurons from the myenteric plexus [Sang and Young, 1996]). Close apposition with Treg cells was observed for both types (Figures 1E and 1F), but particularly for the NOS1$^+$ fibers, somewhat surprisingly given that these fibers are predominantly thought to innervate the muscularis externa (but NOS1$^+$ fibers were clearly seen to radiate into the colonic LP) (Figure S1C).

Because colonic Treg cells fall into major categories, RORγ$^+$ and RORγ$^-$, it was of interest to determine whether both populations were similarly close to neurons. Although RORγ is readily visualized in ILCs and γδT cells, it proved impossible to detect in Treg cells by immunofluorescence or with reporter alleles, so we turned to single-molecule fluorescence *in situ* hybridization (smFISH) (Itzkovitz et al., 2011) with probe libraries detecting *Foxp3* and *Rorc*, counterstained with anti-Tuj1 (Figure 1G). Within *Foxp3*$^+$ cells, we identified those that contained or did not contain *Rorc* transcripts and measured their distance to the closest neuron. Both *Foxp3*$^+$*Rorc*$^+$ cells and *Foxp3*$^+$*Rorc*$^-$ cells were observed at close distances to neurons, exhibiting distributions that were not significantly different (Figure 1H) (chi-sq. $p = 0.58$). Foxp3$^+$ cells therefore exhibited co-localization with neurons regardless of their *Rorc* expression.

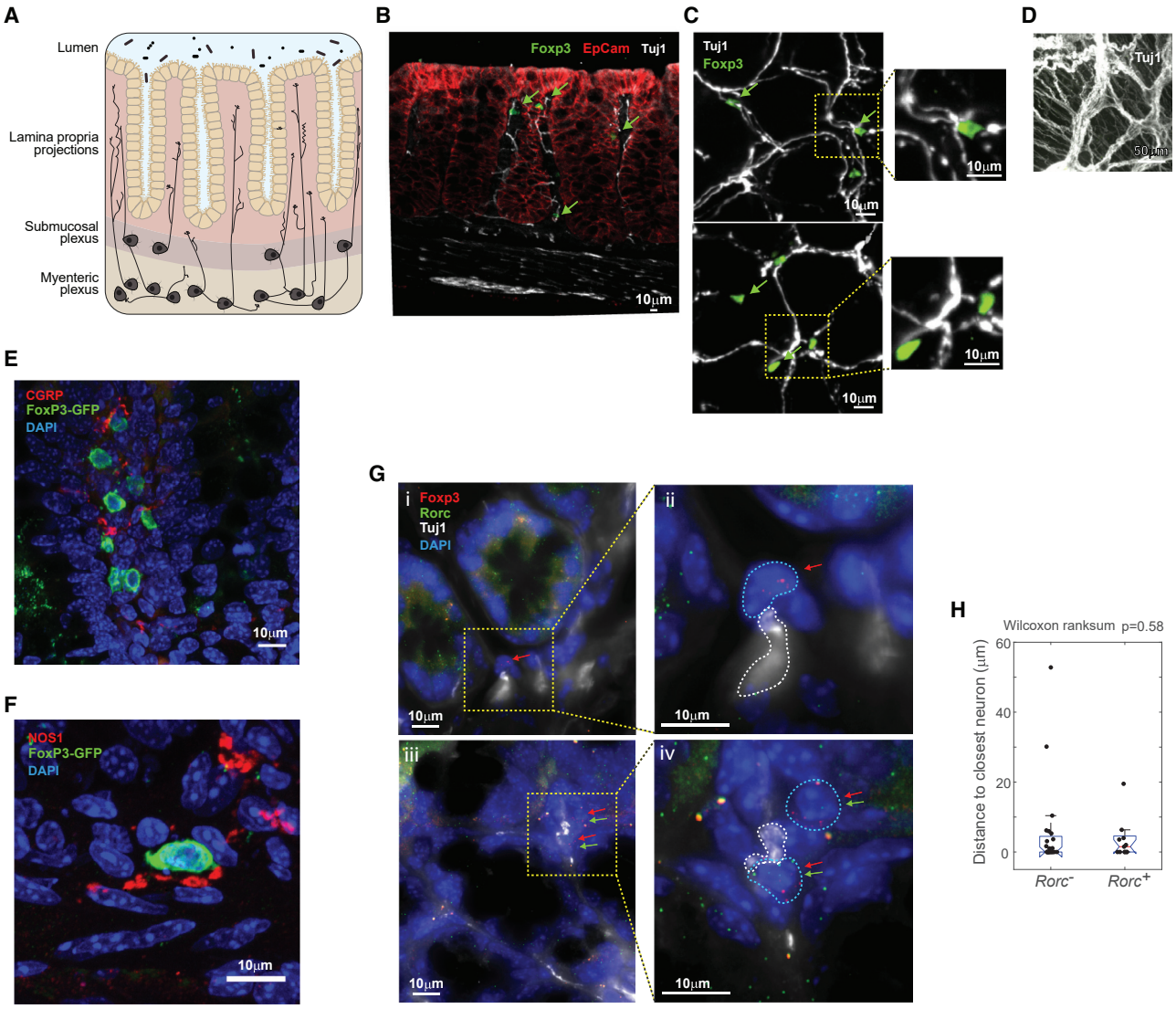

Figure 1. Colonic Treg cells localize closely to neurons

(A) Schematic of the ENS in the colon.

(B) Confocal images of colon cryosections from *Foxp3-gfp* reporter mice immunostained for Tuj1 (white), GFP (green), and EpCAM (red). Arrows indicate GFP$^+$ Treg cells scatted in the lamina propria.

(C and D) Cleared whole-mount of the ENS in colon segments from *Foxp3-gfp* mice, stained for Tuj1 (white) and GFP (green). In (C), Z stacks images (0.5 μm) in the lamina propria, max projection to 5 mm total thickness; in (D) are 35 mm max projections in the myenteric plexus.

(E and F) Confocal images of colon cryosections from *Foxp3-gfp* reporter mice immunostained for Tuj1 (green), CGRP, or NOS1 (red), with DAPI nuclear stain.

(G) smFISH of *Foxp3* mRNAs (red dots) and *Rorc* mRNAs (green dots), counterstained with DAPI (blue, nuclei) and anti-Tuj1 (gray). Examples of *Foxp3*$^+$*Rorc*$^-$ (i and ii) and *Foxp3*$^+$*Rorc*$^+$ (iii and iv) cells in close vicinity to nerve fibers. Images are max projections of 6 stacks (each 0.3 μm apart) for (i) and (iii) and 9 stacks for (ii) and (iv).

(H) Quantification, from smFISH such as (G), of the distances to the closest Tuj1$^+$ cell for 13 *Foxp3*$^+$*Rorc*$^+$ and 21 *Foxp3*$^+$*Rorc*$^-$ cells (p = ns). All data in (A)–(H) is representative of three independent experiments.

Enteric neurons prevent iTreg induction

To explore more directly the functional crosstalk between ENS neurons and Treg cells, we performed co-culture experiments using as a proxy the "iTreg" system, in which FoxP3$^+$ Treg-like cells are induced. The myenteric plexus was dissociated with the surrounding muscle layers (hereafter muscularis myenteric plexus [MMP]), and cells were dissociated and cultured for 3–5 days in "progenitor cell differentiation medium" that supports ENS neurons *in vitro* (Zhang and Hu, 2013). CD4$^+$ T conventional (Tconv) cells were added in a condition known to induce FoxP3 expression (supplementation with anti-CD3$^+$CD28 beads, IL-2, and tumor growth factor-β [TGF-β]). In these co-cultures, enteric neurons inhibited iTreg induction in a dose-dependent manner (Figure 2A). This inhibition was very sensitive, observed with only 1,000 neurons (~1:100 ratio in relation to cultured CD4$^+$ T cells). The inhibition was not due to

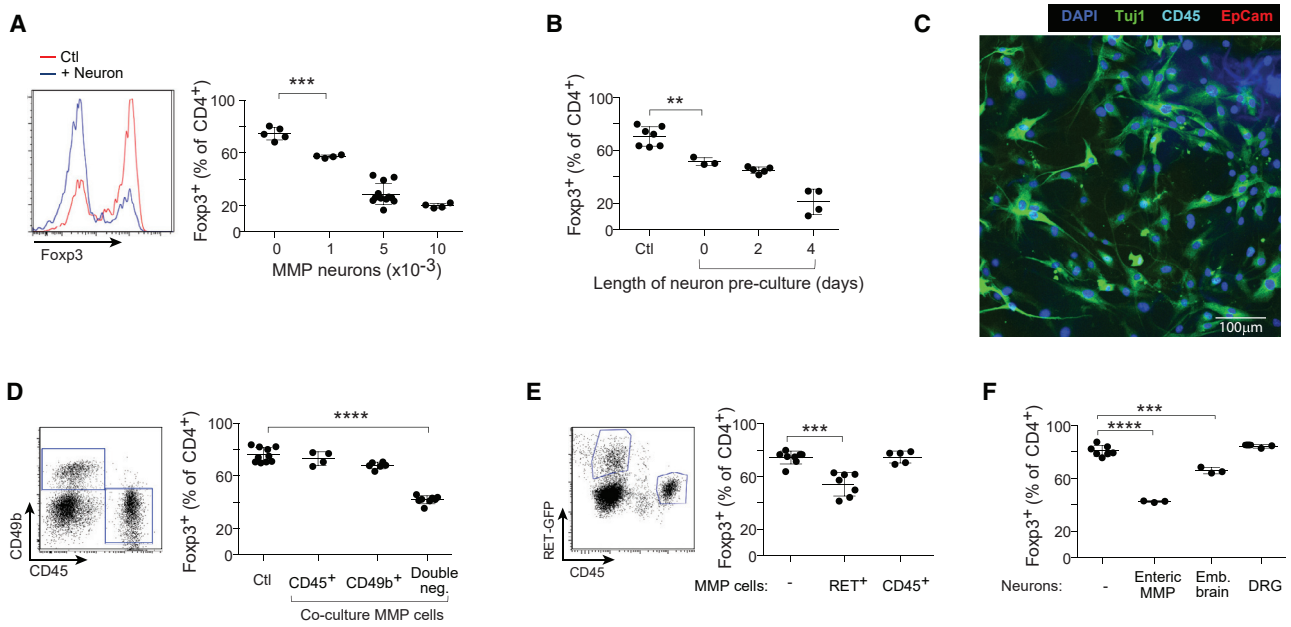

Figure 2. Enteric neurons inhibit iTreg induction

(A) ENS neurons from colon MMP were adapted to culture, then co-cultured along with $CD4^+$ T cells in 72 h iTreg induction cultures, and the effect on induction of FoxP3 assessed by flow cytometry. Shown on the left are representative histograms; on the right is a quantitation of $FoxP3^+$ iTregs in the cultures. Each dot is an independent culture, composite of 3 experiments. Here and thereafter, *$p < 0.05$; **$p < 0.01$; ***$p < 0.001$; ****$p < 10^{-4}$ from unpaired Student's t test unless otherwise specified. Error bars mean ± SD.

(B) As in (A), where MMP neurons were cultured for indicated times before addition to iTreg induction cultures. Composite of three experiments.

(C) Confocal imaging of MMP neuron cultures immunostained for Tuj1, EpCAM (epithelial cells), CD45 (hematopoietic cells), and DAPI (nuclei). Representative of two or more fields in three independent cultures.

(D) $CD45^+$, $CD49b^+$, and $CD45^-CD49b^-$ cell fractions were sorted from dissociated colon MMP (left) and their ability to inhibit iTreg induction tested as in (A). Composite of three experiments.

(E) As in (A), inhibitory cells tested were $CD45^+$ hematopoietic cells or Ret^+ neurons from the MMP of *Ret-gfp* reporter mice. Composite of three experiments.

(F) As in (A), inhibitory cells tested were cultured primary neurons from the MMP, embryonic brain, or DRG. Composite of three experiments.

neuron-induced death, given that the total number of $CD4^+$ T cells dropped only slightly with neuron addition (Figure S2A), and neurons were not toxic to purified *ex vivo* Treg cells in similar cultures (Figure S2B). We also noted that the inhibitory capacity required some degree of adaptation in culture, concurrent with the morphological maturation over 3–5 days observed in the cultures (Figure 2B) (there was no appreciable change in cell numbers over this period).

Several controls were performed to ensure that the inhibition of iTreg differentiation was due to neurons, and not to contaminating cells of another type, like myocytes, hematopoietic cells, or glia. First, fluorescence microscopy showed that, after 3 days, these ENS cultures were positive for Tuj1, and none were positive for markers of epithelial or hematopoietic cells (Figure 2C) (myocytes floated off after a day). Second, we purified the MMP cell suspension by using flow cytometry, separating $CD49b^+$ enteric glial cells (Joseph et al., 2011) and $CD45^+$ hematopoietic cells. Only the double-negative fraction inhibited iTreg appearance (Figure 2D). Third, we used *Ret-gfp* reporter mice, in which only neurons are fluorescent in the MMP (40%∼60% of them) (Jain et al., 2006), sorting $CD45^-GFP^+$ neurons. These were inhibitory, whereas the $CD45^+$ fraction was not (Figure 2E). Thus, we concluded that it was enteric neurons, and not other cell types in these MMP cultures, that inhibited iTreg differentiation.

We then asked whether this inhibitory effect was a general characteristic of neurons. Cultures were prepared with the same numbers (5,000) of embryonic brain neurons, or adult DRG neurons (which include gut-innervating extrinsic sensory afferents). Brain neurons showed a relatively minor inhibitory effect, whereas DRG neurons had no effect, which indicated that the inhibition was not a generic property, ENS neurons having the highest capability (Figure 2F).

Enteric neurons inhibit iTregs through cytokine-like large soluble factors

To determine whether the inhibition by enteric neurons of iTreg required cell-cell contact, we used a Transwell chamber to separate neurons and T cells. Neurons were still inhibitory (Figure 3A). Moreover, supernatants (SNs) from the neuron cultures also had strong inhibitory effects (Figure 3B). Thus, a soluble factor(s) released by neurons in culture played the inhibitory role.

T cells express receptors and are influenced by a number of neurotransmitters or neuropeptides, and these were attractive candidates as secreted inhibitors released by cultured neurons. When such mediators were added to iTreg induction cultures (summarized in Figure 3C; full titrations and cell viability in Figure S3A), most had no detectable inhibitory action, or only at doses that began to induce T cell death (vasoactive intestinal

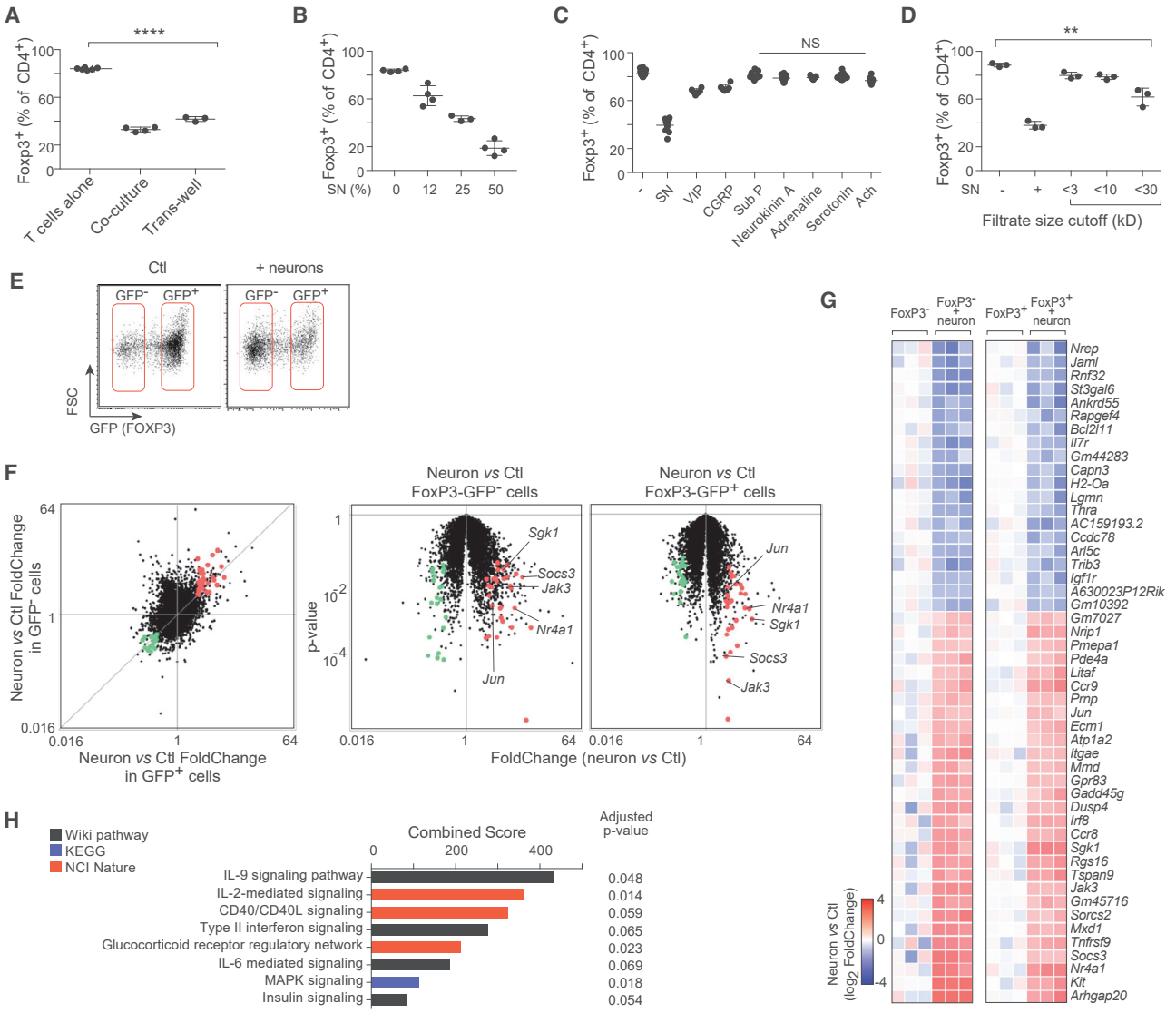

Figure 3. Enteric neurons inhibit iTregs through cytokine-like large soluble factors

(A) Frequency of Foxp3$^+$ cells in 72 h iTreg induction cultures, supplemented with neurons in direct contact or separated in a Transwell chamber. Each dot is an independent culture, composite of three experiments.

(B) As in (A), cultures supplemented with increasing dose of supernatant from 5-day cultures of primary MMP neurons. Composite of two experiments.

(C) As in (B), cultures supplemented with varying doses of neuromediators. Composite of 4 experiments. See Figure S3 for detailed titration curves.

(D) As in (B), cultures supplemented with fractions from molecular weight cutoff filtration. Composite of three experiments.

(E) Representative flow-cytometry sorting gates for 72 h iTreg cultures, alone or supplemented with neurons.

(F) RNA-seq profiling of cells shown in (E). Shown on the left are changes in gene expression induced by the presence of neurons, shown on a "FoldChange/FoldChange" plot, relating in GFP$^+$ iTregs and in non-converted GFP$^+$ cells. Shown on the right is the FoldChange versus p "Volcano plot" showing the significance of neuron-induced changes in Foxp3-GFP$^-$ and Foxp3-GFP$^+$ cells. Transcripts up- or downregulated in T cells by MMP neurons in both cell states (at FC > 2 and p < 0.01) are highlighted (red and green).

(G) Heatmap of changes in the geneset selected in (F) (log_2 of FoldChange in relation to the mean of controls, calculated independently for Foxp3$^-$GFP$^+$ and Foxp3$^-$GFP$^-$ cells; each column is a biological replicate.

(H) Pathway and Gene Ontology analysis of the upregulated transcripts in the signature from (F).

peptide [VIP], CGRP, diethylenetriamine). These data suggested that classic neurotransmitters or neuropeptides might not be the mediators. We then performed a sizing analysis by using centrifugal filters to fractionate the neuronal SNs. Inhibition was absent in small molecular weight fractions and started to be recovered in the filtrates > 30 kD, suggesting that large molecules secreted by enteric neurons, but not small neuropeptides, inhibited iTreg induction (Figure 3D).

For clues to determine the identity of the mediator(s), we analyzed via gene expression profiling the effect of the neurons on differentiating iTreg cells. Co-cultures were set up as above with Tconv cells from *Foxp3-gfp* reporter mice, with or without

neurons. After 72 h, we sorted and profiled by using RNA sequencing (RNA-seq) both neurons and T cells from the cultures. For the latter, we analyzed independently both the green fluorescent protein (GFP)$^+$ and GFP$^-$ populations, in order to factor out shifting frequencies of iTregs (Figure 3E) and to focus on the signals received by the T cells rather than on iTreg differentiation itself. A common set of transcripts induced or repressed by neurons was observed in both GFP$^-$ and GFP$^+$ T cells (Figures 3F and 3G). These induced transcripts included *Jak3* and *Sgk1* (encoding kinases associated with cytokine signaling), *Jun* and *Nr4a1* (encoding early-response TFs), and *Socs3*, which encodes a member of the Suppressor of Cytokine Signaling family typically induced upon cytokine exposure. These findings suggested that neurons were affecting T cells in these cultures through cytokine-like signals. Indeed, pathway and Gene Ontology (GO) analysis revealed that the gene set affected by neurons overlapped with cytokine signaling (Figure 3H).

Enteric neurons prevent Treg induction through IL-6

Given that the data above suggested the involvement of cytokine-like molecules, we performed an interaction analysis and searched these transcriptomes for interacting pairs, where the secreted ligand would be expressed by cultured neurons and the receptors by the T cells (Figure 4A). Several such interactions appeared in the heatmaps ranked by expression intensity: IL-6; leukemia inhibitory factor (LIF); the chemokines CCL2, CCL17, and CXCL12; and the TNF family member TL1A (*Tnfsf15*) were expressed by the cultured neurons, whereas their receptors were present on the CD4$^+$ T cells. Within the nervous system, *Il6*, *Lif*, and *Ccl2* are mostly expressed by cells of the peripheral nervous system, as evidenced by single-cell RNA-seq data (Figure 4B) (Zeisel et al., 2018; www.mousebrain.org). *Il6* was expressed by several enteric neurons, especially the ENT2 nitrergic motor neurons (Figure 4B, inset) whose termini were seen in close contact with LP Treg cells (Figure 1F). To assess the relevance of those candidates, we added antibodies against these protein mediators to SN-supplemented T cell cultures. Of these, only anti-IL-6 was able to revert the inhibition of iTreg differentiation (Figure 4C). We verified that IL-6 was indeed released by enteric neurons in culture (Figure 4D), with an accentuation after a few days of culture that matched the neuronal maturation noted in Figure 2B. We verified that the IL-6 was produced by neuronal cells by using the fractionation strategy of cells from the MMP from *Ret*$^{-gfp}$ reporter mice described above. IL-6 was detected in cultures of GFP$^+$CD45$^-$ cells, but not of CD45$^+$ cells (Figure 4E). Together, these data confirm that the enteric neurons were the source of IL-6 in this system.

The effect of IL-6 was not surprising per se, given its known impact on iTreg differentiation (Bettelli et al., 2006; Zhou et al., 2008), but its origin was more surprising because it is commonly thought of as an inflammatory cytokine produced by myeloid or mesenchymal cells (Hunter and Jones, 2015). We used genetic approaches to further ascertain the role of IL-6. First, ENS neurons were prepared from IL6-deficient mice (Kopf et al., 1994). These neurons elicited less inhibition of iTreg induction than did SN from wild-type littermates (Figure 4F). Conversely, T cells harboring deficiencies in the alpha chain of the IL6 receptor, or in the STAT3 signal transducer, were largely refractory to inhibition (Figures 4G and 4H). These data confirmed that IL6 was the major factor through which enteric neurons prevent iTreg induction. In both of these experiments, however, some degree of iTreg inhibition was still present in spite of the elimination of the IL6-Il6R-STAT3 axis, indicating that, in addition to IL6, a secondary mediator made by neurons also downregulates iTreg differentiation.

Enteric neurons modulate RORγ$^+$ Treg induction via IL-6

IL6 is involved in the differentiation of RORγ$^+$ Treg in the gut (Sefik et al., 2015; Eberl and Littman, 2004; Yissachar et al., 2017; Pratama et al., 2020). This major gut Treg subset is influenced by microbes, and we showed previously that the ability of bacterial strains to induce RORγ$^+$ Treg cells correlated with their ability to trigger neuronal activity (Yissachar et al., 2017). It was thus of interest to determine whether the effect of neurons on iTreg differentiation also influenced the proportion of RORγ$^+$ Treg cells in these cultures. The iTreg induction protocol used in the previous experiments did not lead to any detectable expression of RORγ (not shown), so we used an alternative protocol (Wheaton et al., 2017) (anti-CD3 presented by splenic presenting cells) in which RORγ$^+$ Treg cells can differentiate. Added neurons led to a strong inhibition of total FoxP3 induction, as in the previous cultures, but also to the appearance of RORγ$^+$ Treg cells at intermediate neuron numbers (Figure 5A). Neuronal SNs had similar effects (Figure S4). Wheaton et al. (2017) showed that IL-6 influences the outcome in their cultures. To assess whether the effect of neurons could be entirely explained by IL-6, we measured via ELISA the concentration of IL-6 in neuron SNs and in a batch of recombinant IL-6 and performed parallel cultures with matching doses of IL-6. Addition of recombinant IL-6 and matched neuronal SNs showed mirror-like trends (Figure 5B), indicating that IL-6 was the dominant driver of the neuronal effect. There was a dose-dependent relationship between its effects on total Treg cells versus RORγ$^+$ proportions: both shut down at higher doses, but RORγ$^+$ Treg cells numerically increased in the intermediate dose range (Figure 5C). Moreover, quenching of IL-6 in the neuronal SNs by antibodies (Figure 5D) or using SNs prepared from IL-6-deficient mice (Figure 5E) abrogated the effects on both total and RORγ$^+$ Treg cells. The inhibitory effect was not completely eliminated by either genetic ablation or antibody blockade of IL-6, confirming that a second molecule released by neurons can also inhibit iTreg differentiation, albeit far less efficiently than IL-6, and apparently without the RORγ-inducing capacity.

Microbial effect on the neuron-Treg axis

Commensal gut microbes like *Clostridium ramosum* are potent inducers of RORγ$^+$ Treg cells, in a manner that correlates with their ability to trigger neurons *in vitro* (Yissachar et al., 2017), suggesting that these actions could be linked. To connect these dots, we analyzed the effect of mono-colonization of GF mice on ENS structure and composition. Two weeks after mono-colonization with the high-Treg inducer *C. ramosum* or the non-inducer *Peptostreptococcus magnus*, we performed immunofluorescent imaging on whole-mount colon segments as described above (neuron cell bodies identified by antibodies of the pan-neuronal marker HuC/D, nerve fibers by anti-Tuj1). Bacterial colonization induced a strong reduction in the number of

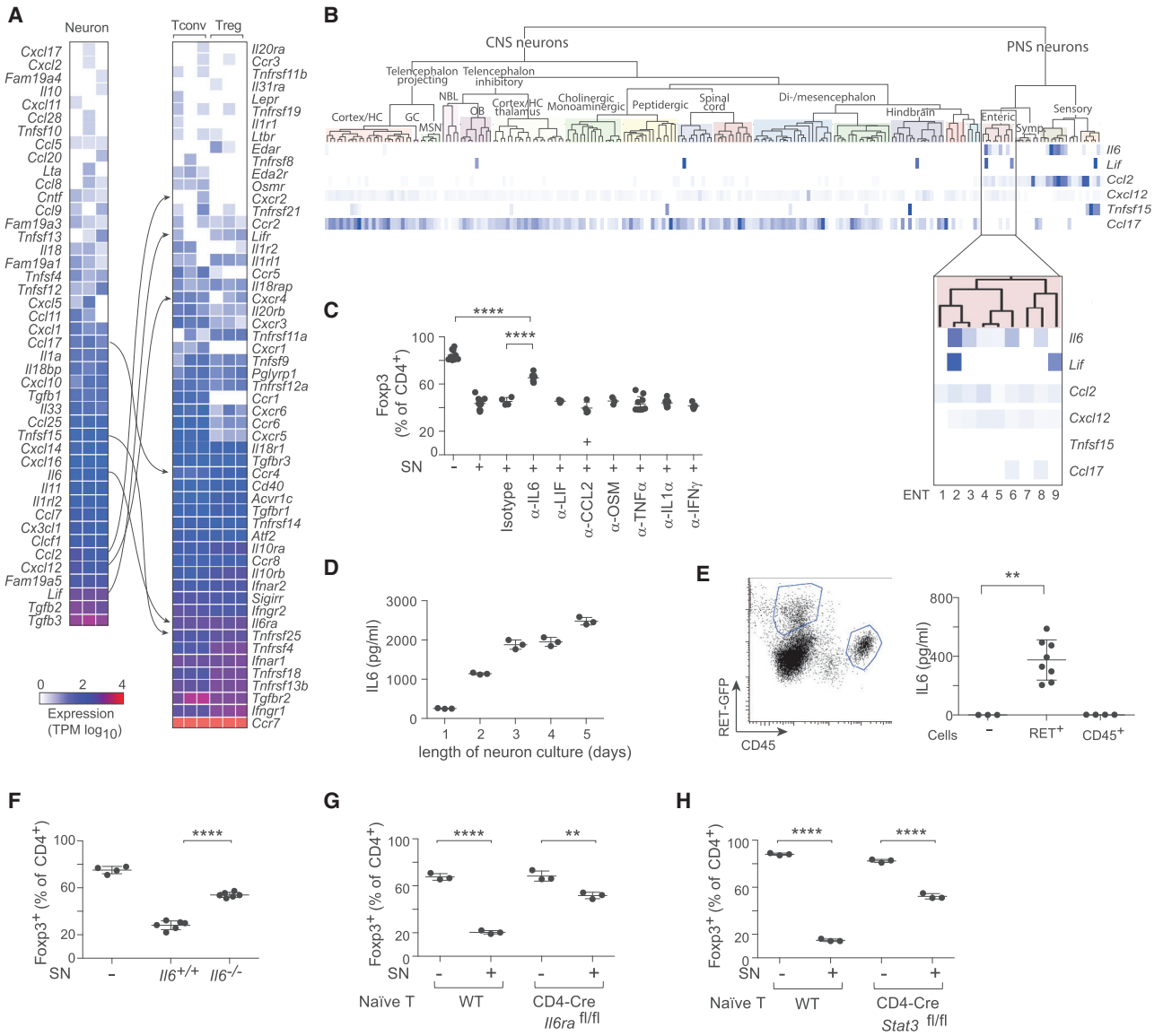

Figure 4. Enteric neurons inhibit iTreg induction through IL-6 pathway

(A) Gene expression results from the neuron/iTreg co-culture from 3E, representing expression values of transcripts encoding large secreted molecules by MMP neurons (left) and surface receptors by T cells (right). Interaction pairs are indicated. Each column is a biological replicate.

(B) Expressions of candidate ligands identified in (A) in different types of enteric neurons defined by Zeisel et al., (2018) (picture generated at www.mousebrain.org).

(C) The frequency of FoxP3$^+$ cells was assessed in 72 h iTreg cultures supplemented from the start with enteric neuron SN, alone or with antibodies (5 ug/mL) against the candidate cytokines identified in (B). Each dot is an independent culture, composite of four experiments.

(D) IL-6 levels (ELISA) in neuronal SNs after different times in culture. Each dot is an independent culture, composite of two experiments.

(E) IL-6 levels (ELISA) in SNs of sorted RET$^+$ and CD45$^+$ populations cultured for 5–7 days. Each dot is an independent culture, composite of three experiments.

(F) Frequency of Foxp3 in iTreg cultures supplemented with neuronal SNs from *Il6*$^{-/-}$ or control littermates. Each dot is an independent culture, composite of three experiments.

(G) Frequency of Foxp3 in iTreg cultures with *Il6ra*-deficient CD4$^+$ T cells (from *Cd4-Cre Il6ra*$^{fl/fl}$ mice) or control littermates supplemented with neuronal SNs. Each dot is an independent culture, composite of three experiments.

(H) As in (G), with input T cells from *Stat3*-deficient mice or control littermates. Composite of three experiments.

neuronal cell bodies and caliber of nerve fiber tracts in the myenteric plexus Figures 6A and 6B), and the density of nerve projections to the LP (Figures 6C and 6D). These changes were strongest after colonization with *C. ramosum*, more modest with *P. magnus.*

We turned to RNA-seq to confirm and analyze temporally the changes to enteric neurons imparted by mono-colonization with these commensal microbes. First, whole MMP from GF and microbe-colonized colons (24 h after colonization) were dissected and profiled via RNA-seq (Figure 6E). Changes

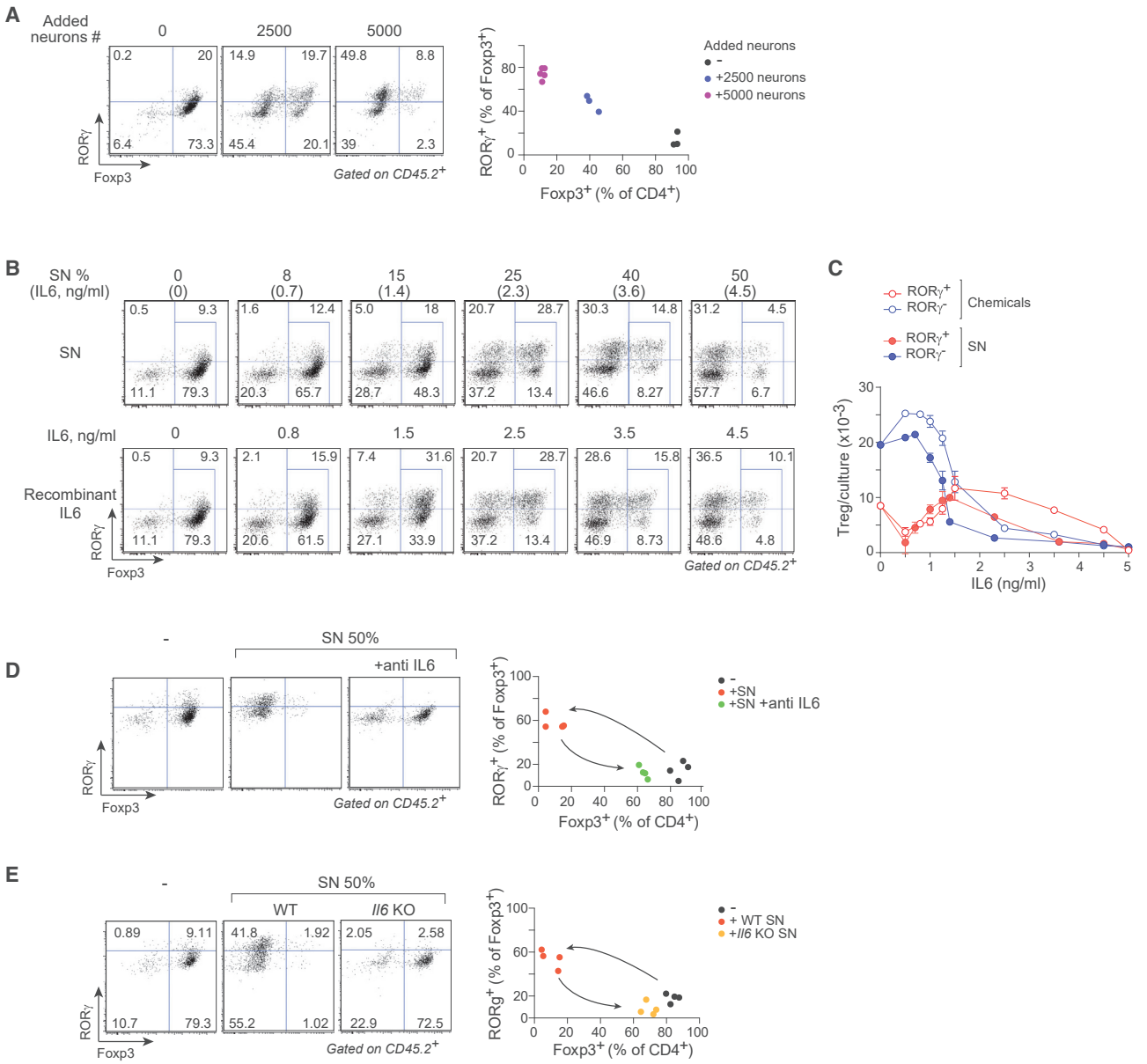

Figure 5. Enteric neurons modulate RORγ$^+$ Treg induction through IL-6

(A) Representative flow-cytometry profiles after 72 h of iTreg cultures (soluble αCD3 + splenic APCs) stained for FoxP3 and RORγ. Each dot is an independent culture. Plot at right compiled from three independent experiments.

(B) Comparison of MMP neuron SNs and recombinant IL-6. Shown on top are iTreg cultures (soluble αCD3 + splenic APCs) supplemented with titrated neuronal SNs in which IL-6 concentration had been pre-determined by ELISA. Shown at the bottom are parallel cultures supplemented with matching concentrations of rIL6 (after ELISA determination). Representative of two independent experiments.

(C) Data from (B), plotting numbers of RORγ$^+$ and RORγ$^-$ Treg cells in iTreg cultures (soluble αCD3 + splenic APCs) supplemented with titrated amounts of neuron supernatant or recombinant IL-6. Each dot is the average value of two or more independent preparations, plot compiled from two independent experiments.

(D) Representative flow-cytometry profiles of iTreg cultures (soluble αCD3 + splenic APCs) supplemented with MMP neuronal SNs and anti-IL-6 (Each dot is an independent culture, compiled data from three independent experiments plotted at right).

(E) As in (D), where the neuron culture SNs was from IL-6-deficient mice or control littermates. Compiled data from three independent experiments plotted at right.

were relatively limited (only 18 transcripts induced or repressed at fold change [FC] > 2 and t test $p < 0.01$), but there was a clear decrease in *Tubb3* and in a set of neurotransmitter-encoding transcripts that we had previously found to be downregulated in whole colon tissue after microbial exposure in organotypic cultures (Yissachar et al., 2017): *Nos1*, *Calcb* (which encodes CGRP-β), *Vip* (which encodes VIP), and *Tac1* (which encodes Substance P and Neurokinin A). These early effects confirmed *in vivo* the significance of our prior *in vitro* data, were concordant with the reduction in neural density seen by

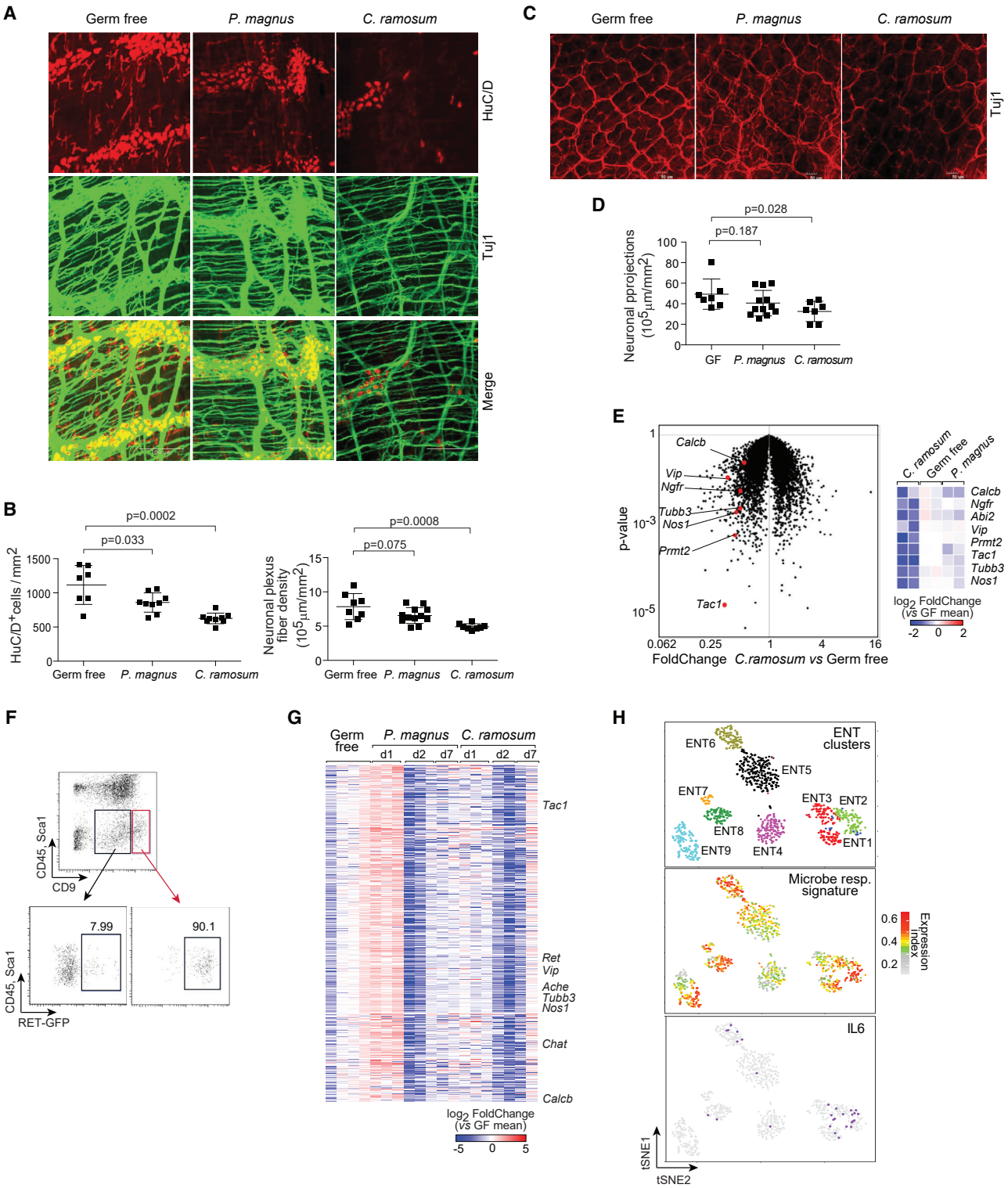

Figure 6. Commensal microbes affect neurons and their phenotypes

(A) Whole-mount staining and quantification of the myenteric plexus in colon segments in GF, *C. ramosum*- or *P. magnus* mono-colonized mice immunostained for Tuj1 (neuronal bodies and fibers, green) and HuC/D (neuron cell bodies, red). Images are max projections of 50–100 stacks (each 0.5 µm apart). Images representative of four independent experiments, and five or more monocolonized mice.

(B) Quantitation (Imaris software) of neuronal body (left) and fiber (right) densities in myenteric plexus from images as in (A). Each dot represents a mouse, composite from four imaging experiments.

(legend continued on next page)

imaging, and suggested that various types of neurons were affected.

To profile the neuronal component more specifically, we then established a flow-cytometric protocol for ENS neuron purification. The colonic MMP was dissected, cells were released by digestion and were stained with antibodies to CD45 (to exclude muscularis macrophages and hematopoietic cells), Sca1 (to exclude mensenchymal cells), and CD9 (which stains many enteric neurons, consistent with small intestine data in mousebrain.org). In pilot experiments performed on *Ret*$^{GFP/+}$ mice, RET^{+} neurons were found mainly in the CD45^{-}Sca1^{-}CD9^{hi} component (Figure 6F). We used this gating strategy to sort for RNA-seq profiling neurons from *C. ramosum* or *P. magnus* mono-colonized GF mice at days 1, 2, and 7 after colonization. Parsing the temporal evolution of the transcripts identified one major coherent cluster of co-varying transcripts. This cluster showed a marked downregulation in response to both bacteria after 2 days, with some recovery after one week, and included many of the neurotransmitter transcripts mentioned above (Figure 6G). This cluster included a number of transcripts typical of different neuron classes, suggesting a widespread effect. To further this point, we mapped the normalized and integrated expression of genes of this cluster onto the single-cell RNA-seq profiles of small intestinal neurons from (Zeisel et al., 2018). The t-distributed stochastic neighbor embedding (tSNE) projection of Figure 6H, top, demarcates the different ENT subsets. The microbe-responsive gene cluster was differentially expressed in ENT subsets, strongest in ENT2 nitrergic neurons (Figure 6H, middle), superimposing well with IL-6 production in ENT2, ENT3, and ENT6 (Figure 6H, bottom). Thus, gene expression affected by microbes affects a wide variety of effectors in ENS neurons, but with some specificity as well.

In these profiles, *Il6* transcripts did not vary at the early time points when neurotransmitters were affected, but were markedly reduced 7 days after colonization by both microbes, whether or not they are RORγ^{+} Treg inducers (Figure 7A). This delay suggested that microbes did not alter neuron-secreted IL-6 directly, but as an outcome of neuronal perturbation. We tested this relationship by comparing colonic Treg populations in genetically engineered mice. First, with mice deficient in several of the affected neurotransmitters, increases in the proportions of total colonic Treg cells were observed in *Vip*- and *Calca*-deficient mice in relation to control littermates, with little or no effect for *Calcb* deficiency (consistent with its low expression in our ENS neuron profiling data) (Figure 7B). None of the mutations affected RORγ^{+} Treg proportions, however (Figure S5). Accordingly, culture SNs of myenteric neurons from *Vip*- and *Calca*-deficient mice were less inhibitory to Treg differentiation than those of littermates, with no effect of *Calcb* deficiency (Figure 7C), reflecting their capacity to produce IL-6 in culture (Figure 7D). Second, we generated mice with neuron-specific deficiency in IL-6, crossing the *Il6*$^{fl/fl}$ allele to *Nestin-Cre* and *Syn1-Cre* driver transgenes (Tronche et al., 1999; Zhu et al., 2001). Specificity was shown by reduced IL-6 production in MMP neuron cultures, but not in LPS-stimulated spleen and muscle used as a control for potential inactivation in myeloid cells (Figures 7E and 7F), and in the ability to repress iTreg differentiation *in vitro* (Figures 7G and 7H) . Most importantly, and providing cell-intrinsic validation of the importance of neuronal IL-6, both crosses showed partial but significant increases in colonic Treg proportions, and decreases in the fraction of RORγ^{+} Treg (Figures 7I and 7J). Together, these results established a connection between gut microbes, VIP and CGRP signaling within the ENS, and Treg differentiation *in vivo* and *in vitro*, one that revolves around IL-6.

DISCUSSION

This work establishes the existence of a triangular crosstalk between gut microbiota, enteric neurons, and Treg cells, an interaction that affects the vertices of the triangle and modulates homeostatic settings. Treg cells lined enteric neuron projections in the LP, enteric neurons affected iTreg induction *in vitro*, commensal microbes strongly and widely affected ENS structure and transcriptome, and genetic perturbations of the ENS affected colonic Treg frequencies. A recurring theme proved to be the production of IL-6 by neurons, a lead anchored by the conditional genetic deletion experiments.

A first argument for an interaction between Treg cells and neurons in the colon came from the close apposition of Treg cells with the fibers that innervate the LP—in contrast, Treg cells were virtually absent from the myenteric plexus, unlike macrophages, which are abundant there (Muller et al., 2014; Gabanyi et al., 2016; De Schepper et al., 2018). Neuronal fibers in the LP tend to follow the microvasculature, and the resolution of the whole-mount imaging or FISH sections cannot formally resolve whether these interactions are direct, or via an intermediate as in the case of the muscle, where IL-33-producing mesenchymal stromal cells connect neurons and Treg cells

(C) Whole-mount immunostaining as in (A), but focused on projections in the LP.
(D) Quantitation of fiber density in images as in (C).
(E) GF mice were mono-colonized with *C. ramosum* or *P. magnus* for 1 day, and RNA was prepared from whole MMP (neuronal and muscle layers) for RNA-seq profiling. Shown on the left are changes in gene expression induced by *C. ramosum* versus GF controls, with characteristic neuronal transcripts highlighted. Shown on the right is a heatmap representation of changes (log_2) versus mean of GF controls, in all replicates.
(F) Gating strategy to sort MMP neurons (CD45^{-}Sca1^{-}CD9^{hi}) from *C. ramosum* or *P. magnus* mono-colonized GF mice for RNA-seq. Bottom panels display RET-GFP expression in MMP from *Ret* $^{GFP/+}$ mice used to establish the strategy then applied to wild-type GF mice.
(G) Changes in gene expression in sorted neurons (gated as in F) for transcripts of the major co-regulated cluster, at different times after mono-colonization with *P.magnus* and *C. ramosum*. (log_2 of FoldChange relative to the mean of GF; clustered by gene-gene correlation within the cluster; each column represents a different mouse). Hallmark neuronal genes indicated.
(H) Differential expression across enteric neurons of the cluster of genes affected by bacterial colonization. Shown on top is a single-cell RNA-seq of small intestinal ENS from (Zeisel et al., 2018), neurons clustered and positioned using tSNE coordinates from that study. Shown in the middle is the normalized expression index for the microbe-responsive cluster (genes from G, expression of each gene normalized to its mean expression across all cells, then all genes summed for each cell) on those cells. Shown on the bottom is the superimposition of *Il6*$^{+}$ cells on the same tSNE.

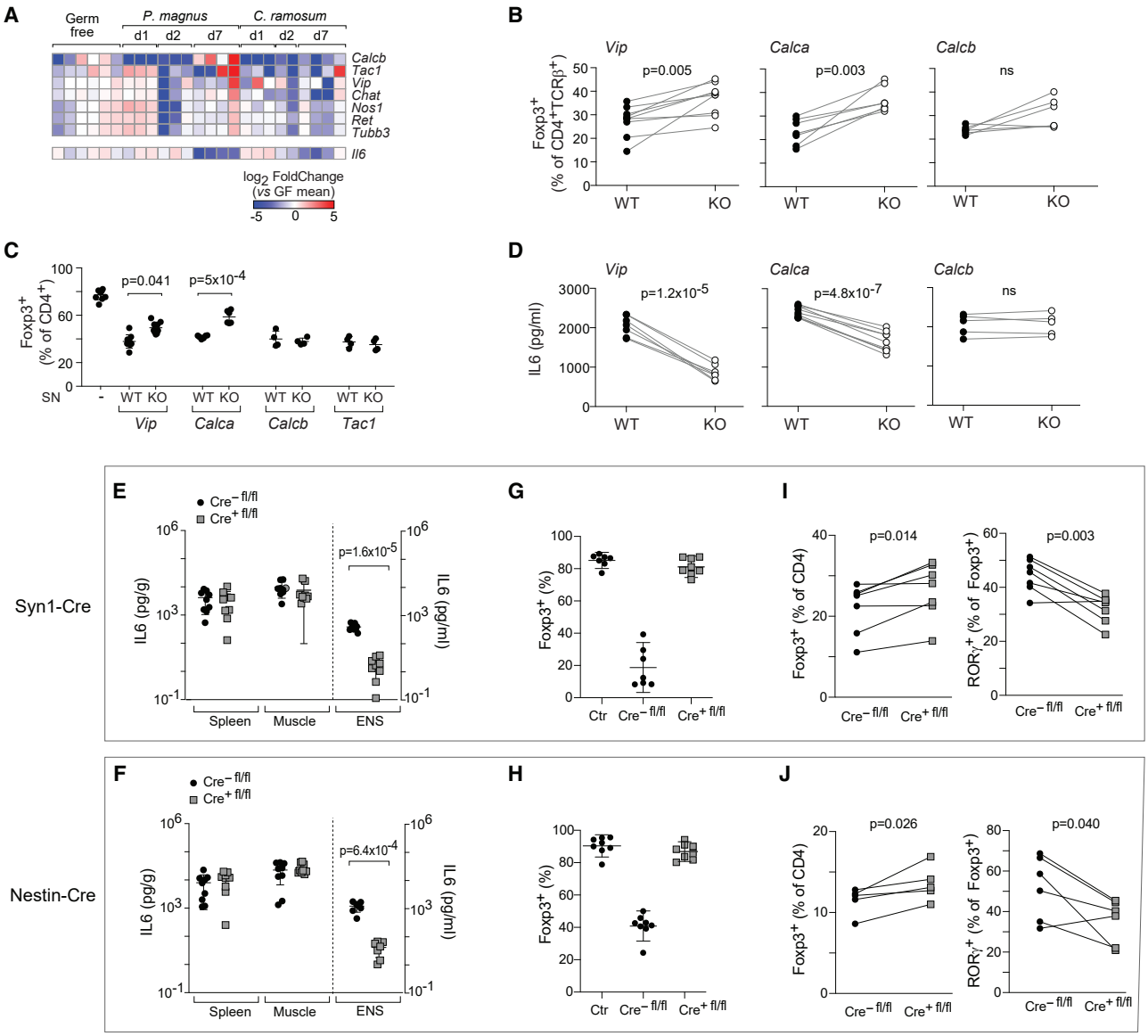

Figure 7. Genetic or microbial changes in neuronal IL-6 affect Treg differentiation *in vivo*

(A) Expression of *Il6* in sorted neurons during the mono-colonization time-course experiment of Fig. 6G. Neurotransmitter transcripts repeated for reference.

(B) Frequency of colonic Treg cells within CD4$^+$ T cells in *Vip*$^{-/-}$, *Calca*$^{-/-}$, *Calcb*$^{-/-}$ mice or control littermates.

(C) iTreg induction cultures were supplemented with neuronal SNs (25%) produced by cultured MMP from *Vip*$^{-/-}$, *Calca*$^{-/-}$, *Calcb*$^{-/-}$, or *Tac1*$^{-/-}$ mice or their wild-type littermates. Each dot is an independent culture, composite of three experiments.

(D) IL-6 levels (ELISA) in neuronal SNs from *Vip*$^{-/-}$, *Calca*$^{-/-}$, or *Calcb*$^{-/-}$or their wild-type littermates.

(E and F) IL-6 levels in MMP neuronal SNs from *Syn1-Crell6*$^{fl/fl}$ (E) and *Nestin-Crell6*$^{fl/fl}$ (F) or their control littermates (mostly cre-negative). LPS-stimulated (100 ng/mL, overnight) whole spleen or muscle cultures used as a control.

(G and H) MMP neurons from *Syn1-Crell6*$^{fl/fl}$ (G) and *Nestin-Crell6*$^{fl/fl}$ (H) or their wild-type littermates were adapted to culture, then co-cultured along with CD4$^+$ T cells in 72 h iTreg induction cultures, and the effect on induction of FoxP3 assessed by flow cytometry. Each dot is an independent culture, composite of three or more experiments.

(I and J) Frequency of colonic Treg cells and RORγ$^+$ Treg cells within CD4$^+$ T cells in *Syn1-Crell6*$^{fl/fl}$ (I) and *Nestin-Crell6*$^{fl/fl}$ (J) or wild-type control littermates. Throughout, each dot represents an individual mouse unless mentioned, p value from paired Student's t test.

(Kuswanto et al., 2016). Colonic RORγ$^+$ and RORγ$^-$ Treg cells differ in their responsiveness to IL-33 (only the latter expressing the IL-33 receptor), but both are found in contact with nerve fibers, suggesting that IL-33 is not as dominant an intermediate in the gut as it is in the muscle. Interestingly, the functional data showed the effect of neuronal IL-6 on the differentiation of iTregs, whereas the images of close apposition between Treg cells and nerve fibers suggest interactions involving differentiated FoxP3$^+$ Treg cells, suggesting neuron-Treg cross-talk at different stages.

Neurons, and especially enteric neurons, inhibited iTreg induction in two different iTreg induction protocols. They also increased the proportion of RORγ$^+$ Treg cells, implying that neurons might have complex dose-dependent effects on the representation and balance of the two Treg populations in the colon. Rather than a non-specific effect of cultured neurons (e.g., Wallerian degeneration), a string of mechanistic and biochemical analyses proved that a defined cytokine, IL-6, proved to be the major mediator of this effect. IL-6 is one of the main inflammatory cytokines, with pleiotropic functions and effects on various immunocytes (Hunter and Jones, 2015). Discovering it in this context was both surprising and unsurprising. IL-6 was unsurprising in this role because it is known to inhibit iTreg differentiation (Bettelli et al., 2006; Zhou et al., 2008), and is needed for normal RORγ$^+$ Treg frequencies in the colon (Sefik et al., 2015; Eberl and Littman, 2004; Yissachar et al., 2017; Pratama et al., 2020). But finding IL-6 was surprising because it had not been previously considered as a mechanism used by neurons to influence the immune system. Documented instances of control of immune cells by the nervous system tend to involve small neuromediators like CGRP, NMU, serotonin, or β-adrenergic agonists (de Jong et al., 2015; Wallrapp et al., 2017; Wallrapp et al., 2019; Klose et al., 2017; Pinho-Ribeiro et al., 2018; Cardoso et al., 2017; Gabanyi et al., 2016). One precedent is the cytokine CSF1, which is secreted by myenteric neurons and promotes the growth of local macrophages (Muller et al., 2014). IL-6 has some recognized roles in the CNS, affecting synaptic transmission and plasticity, with behavioral and cognitive consequences (reviewed in Gadient and Otten, 1997 and Gruol, 2015). Both glia and neurons in the CNS can secrete IL-6 (März et al., 1998; Ringheim et al., 1995), but single-cell RNA-seq revealed an enrichment of *Il6* transcripts in peripheral neurons (Zeisel et al., 2018), especially in enteric and sensory neurons, and we confirmed here that *Il6* is expressed in purified neurons of the myenteric plexus. Although IL6 is the dominant mediator of neuronal inhibition of iTreg induction, one or more other molecules must also be involved: genetic inactivation of *Il6ra* in the T cells (or *Il6* in the neurons) largely, but not completely, abolished the neurons' inhibitory effect. Nor did antibody blockade. The IL-6 family member LIF made a plausible candidate because it is highly expressed in cultured neurons, but anti-LIF antibody failed to block iTreg inhibition, leaving the identity of this second mediator mysterious.

We found that the ENS neurons' ability to produce IL-6 was reduced by inactivation of the important neuropeptide-encoding genes, *Vip* and *Calca* (less so for *Calcb*), with corresponding effects on Treg frequencies *in vivo*. ENT2, nitrergic motor neurons that express *Nos1* and *Vip*, might not have been expected to innervate the LP, but we did observe a strong representation of NOS1$^+$ fibers there, some in close contacts with Treg cells. There was thus consistency between the imaging and transcriptome data, which hints that ENS motor neurons might have additional and unrecognized roles related to immune cell cross-talk (IL-6 was also detected in motor-neuron populations in a recent single-cell atlas of the ENS [Drokhlyansky et al., 2020]). On the other hand, *Calca* is primarily expressed in peptidergic sensory neurons of the DRG, and to a much lower extent in the ENS (Mulderry et al., 1988; Zeisel et al., 2018; Drokhlyansky et al., 2020). These DRG cells were naturally absent from our ENS cultures, suggesting that the effect of the *Calca* deficiency on IL-6 secretion might be indirect. DRG neurons expressing CGRP send their projections to the myenteric plexus (Lai et al., 2020) and might regulate neuron function via RAMP1/CALCRL, the receptor complex for CGRP that is expressed by most enteric neurons (Zeisel et al., 2018). Thus, CGRP from sensory neurons might deliver signals in enteric neurons that are necessary for proper *Il6* expression. More generally, an integrated perspective of the results might simply be that the neuronal release of IL-6 in the colon requires an intact and fully connected ENS and that perturbations in signals from the extrinsic (*Calca* in the DRG) or intrinsic (*Vip* in the ENS) nervous systems perturb this harmonious integration. In keeping, both *Calca*$^{-/-}$ and *Vip*$^{-/-}$ mice have increased susceptibility to colitis (Engel et al., 2012; Wu et al., 2015), which one might speculate to be linked to the neuronal control of Treg cells.

Finally, the effect of commensal microbes on the ENS provides the third side of the triangle. In keeping with the downregulation of neurotransmitter transcripts induced by commensals in the organotypic culture system *in vitro* (Yissachar et al., 2017), the introduction of commensals to the gut of adult GF mice, especially of the RORγ$^+$ Treg inducer *C. ramosum*, led to a rapid decrease of neuronal transcripts in the whole myenteric plexus and to a diminution of the total ENS density over a two-week period. Neuronal *Il6* expression also decreased, but later, consistent with the notion that it is tuned by ENS integrity. Neurons can directly sense bacteria through detection of lipopolysaccharides (LPS), bacterial N-formylated peptides, or pore-forming toxins (Chiu et al., 2013; Meseguer et al., 2014; Pinho-Ribeiro et al., 2018). We propose that the early downregulation upon microbial exposure results as a negative feedback from activation, through sensory receptors or the action of microbial metabolites, of an ENS previously "naive" to microbial input. It is important to note that the loss seemed to affect all neuronal types, as evidenced by the reduction of several specific marker transcripts like *Nos1*, *Tac1*, or *Chat*, which together cover a large proportion of enteric neurons, indicating that the effects are not limited to sensory neurons. It might occur through cell death resulting from over-excitation, or a more subtle retuning of ENS homeostasis.

Both RORγ$^+$-Treg-inducing and non-inducing species depressed IL-6 production. Recall, however, that several signaling pathways from microbes might speak to RORγ$^+$ Treg cells, whether lipid or polysaccharide components (e.g., Arpaia et al., 2013; Hang et al., 2019; Verma et al., 2018), as also modulated by immunoglobulin A (IgA) Ramanan et al., 2020). Thus, although neuron-produced IL-6 is a significant tuner of colonic Treg pools, it does not represent the totality of local Treg homeostasis control, and we hypothesize that *P. magnus* is missing one of the other components required for efficient Treg induction.

Neurons and IL-6 showed a complex relationship between its effects on total Treg cells and on the RORγ$^+$ fraction: lowering total iTregs and boosting the RORγ$^+$ fraction at low concentrations, but blocking both at high concentrations, as relative proportions and absolute cell numbers. This dose-dependence might contribute to the different outcomes of colonization of GF mice with *C. ramosum* and *P. magnus*, which showed different abilities to induce total Treg cells and RORγ$^+$ representations and to downregulate neurons. We should stress, though, that we do not suggest here that neuronal IL-6 is the sole driver of

the induction of RORγ$^+$ Treg cells by gut commensals, given that good evidence has been provided for a role of several bacterially derived products (Verma et al., 2018; Yissachar et al., 2017; Hang et al., 2019; Song et al., 2020). Rather, we propose that the neuronal influence modulates the outcome, amplifying the consequences of bacterially derived triggers, and providing a system-wide integration that the local effect of microbial molecules might not achieve.

Altogether, this study defines a triangular mode of interaction among enteric neurons, Treg cells, and gut microbes, where the nervous system uses IL-6 to tune immunoregulatory tone. One implication is that environmental or genetic perturbation in any one of these poles (microbial dysbiosis, extrinsic neuronal influences, or immune-modulators) might alter the three-way equilibrium and change how tolerance to food or microbes is enforced, modulating the host-microbe interface and the course of inflammatory bowel diseases.

LIMITATION OF STUDY

This study identifies neuronal IL-6 as a strong mediator of the neuron-Treg crosstalk, but IL-6 is not the sole molecular player: either *in vitro*, where we could not identify the minor mediator of IL-6-independent neuronal inhibition of iTreg differentiation or *in vivo*, where inactivation of neuronal *Il6* expression only partially affects Treg numbers and phenotypic balance. The effect of *Vip* and *Calca* ablation were also partial, and it would be interesting to determine mechanistically how their loss affects neuronal IL-6 production. Although neuron-derived IL-6 is clearly important, we do not know how it integrates with other sources of IL-6 in the gut (conditional inactivation in all cells except neurons?), and whether its effect extends beyond Treg cells. It will be important to define the relevance of neuronal IL-6 to inflammatory or autoimmune diseases, how its influence evolves in inflammatory backdrops, and whether it operates in other organismal locations.

STAR★METHODS

Detailed methods are provided in the online version of this paper and include the following:

- KEY RESOURCES TABLE
- RESOURCE AVAILABILITY
  - Lead Contact
  - Materials Availability
  - Data and Code Availability
- EXPERIMENTAL MODEL AND SUBJECT DETAILS
  - Mice
- METHOD DETAILS
  - Germ-free mice (GF) and colonization
  - Enteric neuron cultures
  - Embryonic brain neuron cultures
  - DRG neuron cultures
  - iTreg induction in culture and flow cytometry
  - T/neuron co-cultures
  - RNaseq profiling
  - Flow cytometric analysis
  - Microscopy
  - Fluorescence *in situ* hybridization
- QUANTIFICATION AND STATISTICAL ANALYSIS

SUPPLEMENTAL INFORMATION

Supplemental information can be found online at https://doi.org/10.1016/j.immuni.2021.02.002.

ACKNOWLEDGMENTS

We thank Drs. J. Wheaton, A. Munoz-Rojas, M. Ciofani, D. Kasper, and J. Huh, for insightful discussions and advice; L. Yang, A. Diallo, and C. Yapp (HMS IDAC facility) for help with computational analyses; and A. Jacobson, K. Hattori, N. Lai, A. Louis, and S. Soualhi for mice, advice, and assistance. This study benefited from data posted at mousebrain.org. This work was supported by grants AI125603 to C.B. and D.M., DK110532 to M.R., and AI30019 and AT009499 to I.C. from the NIH; by the JPB Foundation to C.B. and D.M.; by the Broad-ISF exchange to S.I. and C.B. and D.M.; and in part by SRAs from UCB and Evelo Biosciences. D.R. was supported by the Damon Runyon Cancer Research Foundation (DRG 2300-17, National Mah Jongg League Fellow).

AUTHOR CONTRIBUTIONS

Design, Y.Y., M.R., I.C., S.I., M.R., D.M., and C.B.; Experimentation, Y.Y., D.R., M.R., K.M., D.R., O.Y., and T.V.; Computation, Y.Y. and B.V.; Writing, Y.Y., D.R., M.R., and C.B.; review and edits, all.

DECLARATION OF INTERESTS

The authors declare no competing interests.

Received: January 30, 2020
Revised: November 2, 2020
Accepted: February 5, 2021
Published: March 9, 2021

REFERENCES

Al Nabhani, Z., Dulauroy, S., Marques, R., Cousu, C., Al Bounny, S., Déjardin, F., Sparwasser, T., Bérard, M., Cerf-Bensussan, N., and Eberl, G. (2019). A weaning reaction to microbiota is required for resistance to immunopathologies in the adult. Immunity *50*, 1276–1288.e5.

Arpaia, N., Campbell, C., Fan, X., Dikiy, S., van der Veeken, J., deRoos, P., Liu, H., Cross, J.R., Pfeffer, K., Coffer, P.J., and Rudensky, A.Y. (2013). Metabolites produced by commensal bacteria promote peripheral regulatory T-cell generation. Nature *504*, 451–455.

Atarashi, K., Tanoue, T., Shima, T., Imaoka, A., Kuwahara, T., Momose, Y., Cheng, G., Yamasaki, S., Saito, T., Ohba, Y., et al. (2011). Induction of colonic regulatory T cells by indigenous Clostridium species. Science *331*, 337–341.

Bettelli, E., Carrier, Y., Gao, W., Korn, T., Strom, T.B., Oukka, M., Weiner, H.L., and Kuchroo, V.K. (2006). Reciprocal developmental pathways for the generation of pathogenic effector TH17 and regulatory T cells. Nature *441*, 235–238.

Cardoso, V., Chesné, J., Ribeiro, H., García-Cassani, B., Carvalho, T., Bouchery, T., Shah, K., Barbosa-Morais, N.L., Harris, N., and Veiga-Fernandes, H. (2017). Neuronal regulation of type 2 innate lymphoid cells via neuromedin U. Nature *549*, 277–281.

Chen, W., Jin, W., Hardegen, N., Lei, K.J., Li, L., Marinos, N., McGrady, G., and Wahl, S.M. (2003). Conversion of peripheral CD4$^+$CD25$^-$ naive T cells to CD4$^+$CD25$^+$ regulatory T cells by TGF-beta induction of transcription factor Foxp3. J. Exp. Med. *198*, 1875–1886.

Chiu, I.M., Heesters, B.A., Ghasemlou, N., Von Hehn, C.A., Zhao, F., Tran, J., Wainger, B., Strominger, A., Muralidharan, S., Horswill, A.R., et al. (2013). Bacteria activate sensory neurons that modulate pain and inflammation. Nature *501*, 52–57.

de Jong, P.R., Takahashi, N., Peiris, M., Bertin, S., Lee, J., Gareau, M.G., Paniagua, A., Harris, A.R., Herdman, D.S., Corr, M., et al. (2015). TRPM8 on

mucosal sensory nerves regulates colitogenic responses by innate immune cells via CGRP. Mucosal Immunol. *8*, 491–504.

De Schepper, S., Verheijden, S., Aguilera-Lizarraga, J., Viola, M.F., Boesmans, W., Stakenborg, N., Voytyuk, I., Schmidt, I., Boeckx, B., Dierckx de Casterlé, I., et al. (2018). Self-maintaining gut macrophages are essential for intestinal homeostasis. Cell *175*, 400–415.e13.

Drokhlyansky, E., Smillie, C.S., Van Wittenberghe, N., Ericsson, M., Griffin, G.K., Eraslan, G., Dionne, D., Cuoco, M.S., Goder-Reiser, M.N., Sharova, T., et al. (2020). The human and mouse enteric nervous system at single-cell resolution. Cell *182*, 1606–1622.e23.

Eberl, G., and Littman, D.R. (2004). Thymic origin of intestinal alphabeta T cells revealed by fate mapping of RORgammat+ cells. Science *305*, 248–251.

Engel, M.A., Khalil, M., Siklosi, N., Mueller-Tribbensee, S.M., Neuhuber, W.L., Neurath, M.F., Becker, C., and Reeh, P.W. (2012). Opposite effects of substance P and calcitonin gene-related peptide in oxazolone colitis. Dig. Liver Dis. *44*, 24–29.

Furness, J.B., Rivera, L.R., Cho, H.J., Bravo, D.M., and Callaghan, B. (2013). The gut as a sensory organ. Nat. Rev. Gastroenterol. Hepatol. *10*, 729–740.

Furness, J.B., Callaghan, B.P., Rivera, L.R., and Cho, H.J. (2014). The enteric nervous system and gastrointestinal innervation: integrated local and central control. Adv. Exp. Med. Biol. *817*, 39–71.

Gabanyi, I., Muller, P.A., Feighery, L., Oliveira, T.Y., Costa-Pinto, F.A., and Mucida, D. (2016). Neuro-immune interactions drive tissue programming in intestinal macrophages. Cell *164*, 378–391.

Gadient, R.A., and Otten, U.H. (1997). Interleukin-6 (IL-6)–a molecule with both beneficial and destructive potentials. Prog. Neurobiol. *52*, 379–390.

Geva-Zatorsky, N., Sefik, E., Kua, L., Pasman, L., Tan, T.G., Ortiz-Lopez, A., Yanortsang, T.B., Yang, L., Jupp, R., Mathis, D., et al. (2017). Mining the human gut microbiota for immunomodulatory organisms. Cell *168*, 928–943.e11.

Gruol, D.L. (2015). IL-6 regulation of synaptic function in the CNS. Neuropharmacology *96* (Pt A), 42–54.

Hang, S., Paik, D., Yao, L., Kim, E., Trinath, J., Lu, J., Ha, S., Nelson, B.N., Kelly, S.P., Wu, L., et al. (2019). Bile acid metabolites control T_H17 and T_{reg} cell differentiation. Nature *576*, 143–148.

He, Z., Chen, L., Souto, F.O., Canasto-Chibuque, C., Bongers, G., Deshpande, M., Harpaz, N., Ko, H.M., Kelley, K., Furtado, G.C., and Lira, S.A. (2017). Epithelial-derived IL-33 promotes intestinal tumorigenesis in Apc $^{Min/+}$ mice. Sci. Rep. *7*, 5520.

Huh, J.R., and Veiga-Fernandes, H. (2020). Neuroimmune circuits in inter-organ communication. Nat. Rev. Immunol. *20*, 217–228.

Hunter, C.A., and Jones, S.A. (2015). IL-6 as a keystone cytokine in health and disease. Nat. Immunol. *16*, 448–457.

Ibiza, S., García-Cassani, B., Ribeiro, H., Carvalho, T., Almeida, L., Marques, R., Misic, A.M., Bartow-McKenney, C., Larson, D.M., Pavan, W.J., et al. (2016). Glial-cell-derived neuroregulators control type 3 innate lymphoid cells and gut defence. Nature *535*, 440–443.

Itzkovitz, S., Lyubimova, A., Blat, I.C., Maynard, M., van Es, J., Lees, J., Jacks, T., Clevers, H., and van Oudenaarden, A. (2011). Single-molecule transcript counting of stem-cell markers in the mouse intestine. Nat. Cell Biol. *14*, 106–114.

Jain, S., Golden, J.P., Wozniak, D., Pehek, E., Johnson, E.M., Jr., and Milbrandt, J. (2006). RET is dispensable for maintenance of midbrain dopaminergic neurons in adult mice. J. Neurosci. *26*, 11230–11238.

Josefowicz, S.Z., Lu, L.F., and Rudensky, A.Y. (2012). Regulatory T cells: mechanisms of differentiation and function. Annu. Rev. Immunol. *30*, 531–564.

Joseph, N.M., He, S., Quintana, E., Kim, Y.G., Núñez, G., and Morrison, S.J. (2011). Enteric glia are multipotent in culture but primarily form glia in the adult rodent gut. J. Clin. Invest. *121*, 3398–3411.

Klose, C.S.N., Mahlakõiv, T., Moeller, J.B., Rankin, L.C., Flamar, A.L., Kabata, H., Monticelli, L.A., Moriyama, S., Putzel, G.G., Rakhilin, N., et al. (2017). The neuropeptide neuromedin U stimulates innate lymphoid cells and type 2 inflammation. Nature *549*, 282–286.

Kopf, M., Baumann, H., Freer, G., Freudenberg, M., Lamers, M., Kishimoto, T., Zinkernagel, R., Bluethmann, H., and Köhler, G. (1994). Impaired immune and acute-phase responses in interleukin-6-deficient mice. Nature *368*, 339–342.

Kulkarni, S., Ganz, J., Bayrer, J., Becker, L., Bogunovic, M., and Rao, M. (2018). Advances in enteric neurobiology: The "brain" in the gut in health and disease. J. Neurosci. *38*, 9346–9354.

Kuswanto, W., Burzyn, D., Panduro, M., Wang, K.K., Jang, Y.C., Wagers, A.J., Benoist, C., and Mathis, D. (2016). Poor repair of skeletal muscle in aging mice reflects a defect in local, interleukin-33-dependent accumulation of regulatory T cells. Immunity *44*, 355–367.

Lai, N.Y., Musser, M.A., Pinho-Ribeiro, F.A., Baral, P., Jacobson, A., Ma, P., Potts, D.E., Chen, Z., Paik, D., Soualhi, S., et al. (2020). Gut-Innervating Nociceptor Neurons Regulate Peyer's Patch Microfold Cells and SFB Levels to Mediate Salmonella Host Defense. Cell *180*, 33–49.e22.

Lathrop, S.K., Bloom, S.M., Rao, S.M., Nutsch, K., Lio, C.W., Santacruz, N., Peterson, D.A., Stappenbeck, T.S., and Hsieh, C.S. (2011). Peripheral education of the immune system by colonic commensal microbiota. Nature *478*, 250–254.

Liu, Y., Teige, I., Birnir, B., and Issazadeh-Navikas, S. (2006). Neuron-mediated generation of regulatory T cells from encephalitogenic T cells suppresses EAE. Nat. Med. *12*, 518–525.

Margolis, K.G., Gershon, M.D., and Bogunovic, M. (2016). Cellular Organization of Neuroimmune Interactions in the Gastrointestinal Tract. Trends Immunol. *37*, 487–501.

März, P., Cheng, J.G., Gadient, R.A., Patterson, P.H., Stoyan, T., Otten, U., and Rose-John, S. (1998). Sympathetic neurons can produce and respond to interleukin 6. Proc. Natl. Acad. Sci. USA *95*, 3251–3256.

Meseguer, V., Alpizar, Y.A., Luis, E., Tajada, S., Denlinger, B., Fajardo, O., Manenschijn, J.A., Fernández-Peña, C., Talavera, A., Kichko, T., et al. (2014). TRPA1 channels mediate acute neurogenic inflammation and pain produced by bacterial endotoxins. Nat. Commun. *5*, 3125.

Molofsky, A.B., Savage, A.K., and Locksley, R.M. (2015). Interleukin-33 in tissue homeostasis, injury, and inflammation. Immunity *42*, 1005–1019.

Mulderry, P.K., Ghatei, M.A., Spokes, R.A., Jones, P.M., Pierson, A.M., Hamid, Q.A., Kanse, S., Amara, S.G., Burrin, J.M., Legon, S., et al. (1988). Differential expression of alpha-CGRP and beta-CGRP by primary sensory neurons and enteric autonomic neurons of the rat. Neuroscience *25*, 195–205.

Muller, P.A., Koscsó, B., Rajani, G.M., Stevanovic, K., Berres, M.L., Hashimoto, D., Mortha, A., Leboeuf, M., Li, X.M., Mucida, D., et al. (2014). Crosstalk between muscularis macrophages and enteric neurons regulates gastrointestinal motility. Cell *158*, 300–313.

Neumann, C., Blume, J., Roy, U., Teh, P.P., Vasanthakumar, A., Beller, A., Liao, Y., Heinrich, F., Arenzana, T.L., Hackney, J.A., et al. (2019). c-Maf-dependent T_{reg} cell control of intestinal T_H17 cells and IgA establishes host-microbiota homeostasis. Nat. Immunol. *20*, 471–481.

Nutsch, K., Chai, J.N., Ai, T.L., Russler-Germain, E., Feehley, T., Nagler, C.R., and Hsieh, C.S. (2016). Rapid and Efficient Generation of Regulatory T Cells to Commensal Antigens in the Periphery. Cell Rep. *17*, 206–220.

Ohnmacht, C., Park, J.H., Cording, S., Wing, J.B., Atarashi, K., Obata, Y., Gaboriau-Routhiau, V., Marques, R., Dulauroy, S., Fedoseeva, M., et al. (2015). The microbiota regulates type 2 immunity through $ROR\gamma^+$ T cells. Science *349*, 989–993.

Panduro, M., Benoist, C., and Mathis, D. (2016). Tissue Tregs. Annu. Rev. Immunol. *34*, 609–633.

Peine, M., Marek, R.M., and Löhning, M. (2016). IL-33 in T Cell Differentiation, Function, and Immune Homeostasis. Trends Immunol. *37*, 321–333.

Picelli, S., Faridani, O.R., Björklund, A.K., Winberg, G., Sagasser, S., and Sandberg, R. (2014). Full-length RNA-seq from single cells using Smart-seq2. Nat. Protoc. *9*, 171–181.

Pinho-Ribeiro, F.A., Baddal, B., Haarsma, R., O'Seaghdha, M., Yang, N.J., Blake, K.J., Portley, M., Verri, W.A., Dale, J.B., Wessels, M.R., and Chiu, I.M. (2018). Blocking neuronal signaling to immune cells treats streptococcal invasive infection. Cell *173*, 1083–1097.e22.

Pratama, A., Schnell, A., Mathis, D., and Benoist, C. (2020). Developmental and cellular age direct conversion of CD4$^+$ T cells into RORγ^+ or Helios$^+$ colon Treg cells. J. Exp. Med. *217*, e20190428.

Quintana, A., Erta, M., Ferrer, B., Comes, G., Giralt, M., and Hidalgo, J. (2013). Astrocyte-specific deficiency of interleukin-6 and its receptor reveal specific roles in survival, body weight and behavior. Brain Behav. Immun. *27*, 162–173.

Ramanan, D., Sefik, E., Galván-Peña, S., Wu, M., Yang, L., Yang, Z., Kostic, A., Golovkina, T.V., Kasper, D.L., Mathis, D., and Benoist, C. (2020). An immunologic mode of multigenerational transmission governs a gut Treg setpoint. Cell *181*, 1276–1290.e13.

Ringheim, G.E., Burgher, K.L., and Heroux, J.A. (1995). Interleukin-6 mRNA expression by cortical neurons in culture: evidence for neuronal sources of interleukin-6 production in the brain. J. Neuroimmunol. *63*, 113–123.

Sang, Q., and Young, H.M. (1996). Chemical coding of neurons in the myenteric plexus and external muscle of the small and large intestine of the mouse. Cell Tissue Res. *284*, 39–53.

Schiering, C., Krausgruber, T., Chomka, A., Fröhlich, A., Adelmann, K., Wohlfert, E.A., Pott, J., Griseri, T., Bollrath, J., Hegazy, A.N., et al. (2014). The alarmin IL-33 promotes regulatory T-cell function in the intestine. Nature *513*, 564–568.

Schindelin, J., Arganda-Carreras, I., Frise, E., Kaynig, V., Longair, M., Pietzsch, T., Preibisch, S., Rueden, C., Saalfeld, S., Schmid, B., et al. (2012). Fiji: an open-source platform for biological-image analysis. Nat. Methods *9*, 676–682.

Sefik, E., Geva-Zatorsky, N., Oh, S., Konnikova, L., Zemmour, D., McGuire, A.M., Burzyn, D., Ortiz-Lopez, A., Lobera, M., Yang, J., et al. (2015). MUCOSAL IMMUNOLOGY. Individual intestinal symbionts induce a distinct population of RORγ^+ regulatory T cells. Science *349*, 993–997.

Song, X., Sun, X., Oh, S.F., Wu, M., Zhang, Y., Zheng, W., Geva-Zatorsky, N., Jupp, R., Mathis, D., Benoist, C., and Kasper, D.L. (2020). Microbial bile acid metabolites modulate gut RORγ^+ regulatory T cell homeostasis. Nature *577*, 410–415.

Teratani, T., Mikami, Y., Nakamoto, N., Suzuki, T., Harada, Y., Okabayashi, K., Hagihara, Y., Taniki, N., Kohno, K., Shibata, S., et al. (2020). The liver-brain-gut neural arc maintains the T_{reg} cell niche in the gut. Nature *585*, 591–596.

Thompson, B.J., Washington, M.K., Kurre, U., Singh, M., Rula, E.Y., and Emeson, R.B. (2008). Protective roles of alpha-calcitonin and beta-calcitonin gene-related peptide in spontaneous and experimentally induced colitis. Dig. Dis. Sci. *53*, 229–241.

Tronche, F., Kellendonk, C., Kretz, O., Gass, P., Anlag, K., Orban, P.C., Bock, R., Klein, R., and Schütz, G. (1999). Disruption of the glucocorticoid receptor gene in the nervous system results in reduced anxiety. Nat. Genet. *23*, 99–103.

Veiga-Fernandes, H., and Mucida, D. (2016). Neuro-immune interactions at barrier surfaces. Cell *165*, 801–811.

Verma, R., Lee, C., Jeun, E.J., Yi, J., Kim, K.S., Ghosh, A., Byun, S., Lee, C.G., Kang, H.J., Kim, G.C., et al. (2018). Cell surface polysaccharides of *Bifidobacterium bifidum* induce the generation of Foxp3$^+$ regulatory T cells. Sci. Immunol. *3*, eaat6975.

Wallrapp, A., Riesenfeld, S.J., Burkett, P.R., Abdulnour, R.E., Nyman, J., Dionne, D., Hofree, M., Cuoco, M.S., Rodman, C., Farouq, D., et al. (2017). The neuropeptide NMU amplifies ILC2-driven allergic lung inflammation. Nature *549*, 351–356.

Wallrapp, A., Burkett, P.R., Riesenfeld, S.J., Kim, S.J., Christian, E., Abdulnour, R.E., Thakore, P.I., Schnell, A., Lambden, C., Herbst, R.H., et al. (2019). Calcitonin gene-related peptide negatively regulates alarmin-driven type 2 innate lymphoid cell responses. Immunity *51*, 709–723.e6.

Wheaton, J.D., Yeh, C.H., and Ciofani, M. (2017). Cutting Edge: c-Maf Is Required for Regulatory T Cells To Adopt RORγt$^+$ and Follicular Phenotypes. J. Immunol. *199*, 3931–3936.

Wohlfert, E.A., Grainger, J.R., Bouladoux, N., Konkel, J.E., Oldenhove, G., Ribeiro, C.H., Hall, J.A., Yagi, R., Naik, S., Bhairavabhotla, R., et al. (2011). GATA3 controls Foxp3$^+$ regulatory T cell fate during inflammation in mice. J. Clin. Invest. *121*, 4503–4515.

Wu, X., Conlin, V.S., Morampudi, V., Ryz, N.R., Nasser, Y., Bhinder, G., Bergstrom, K.S., Yu, H.B., Waterhouse, C.C., Buchan, A.M., et al. (2015). Vasoactive intestinal polypeptide promotes intestinal barrier homeostasis and protection against colitis in mice. PLoS ONE *10*, e0125225.

Xu, M., Pokrovskii, M., Ding, Y., Yi, R., Au, C., Harrison, O.J., Galan, C., Belkaid, Y., Bonneau, R., and Littman, D.R. (2018). c-MAF-dependent regulatory T cells mediate immunological tolerance to a gut pathobiont. Nature *554*, 373–377.

Yang, N.J., and Chiu, I.M. (2017). Bacterial signaling to the nervous system through toxins and metabolites. J. Mol. Biol. *429*, 587–605.

Yang, B.H., Hagemann, S., Mamareli, P., Lauer, U., Hoffmann, U., Beckstette, M., Föhse, L., Prinz, I., Pezoldt, J., Suerbaum, S., et al. (2016). Foxp3($^+$) T cells expressing RORγt represent a stable regulatory T-cell effector lineage with enhanced suppressive capacity during intestinal inflammation. Mucosal Immunol. *9*, 444–457.

Ye, J., Qiu, J., Bostick, J.W., Ueda, A., Schjerven, H., Li, S., Jobin, C., Chen, Z.E., and Zhou, L. (2017). The aryl hydrocarbon receptor preferentially marks and promotes gut regulatory T cells. Cell Rep. *21*, 2277–2290.

Yissachar, N., Zhou, Y., Ung, L., Lai, N.Y., Mohan, J.F., Ehrlicher, A., Weitz, D.A., Kasper, D.L., Chiu, I.M., Mathis, D., and Benoist, C. (2017). An intestinal organ culture system uncovers a role for the nervous system in microbe-immune crosstalk. Cell *168*, 1135–1148.e12.

Yoo, B.B., and Mazmanian, S.K. (2017). The Enteric Network: Interactions between the Immune and Nervous Systems of the Gut. Immunity *46*, 910–926.

Zeisel, A., Hochgerner, H., Lönnerberg, P., Johnsson, A., Memic, F., van der Zwan, J., Häring, M., Braun, E., Borm, L.E., La Manno, G., et al. (2018). Molecular architecture of the mouse nervous system. Cell *174*, 999–1014.e22.

Zhang, Y., and Hu, W. (2013). Mouse enteric neuronal cell culture. Methods Mol. Biol. *1078*, 55–63.

Zhou, L., Lopes, J.E., Chong, M.M., Ivanov, I.I., Min, R., Victora, G.D., Shen, Y., Du, J., Rubtsov, Y.P., Rudensky, A.Y., et al. (2008). TGF-beta-induced Foxp3 inhibits T(H)17 cell differentiation by antagonizing RORgammat function. Nature *453*, 236–240.

Zhu, Y., Romero, M.I., Ghosh, P., Ye, Z., Charnay, P., Rushing, E.J., Marth, J.D., and Parada, L.F. (2001). Ablation of NF1 function in neurons induces abnormal development of cerebral cortex and reactive gliosis in the brain. Genes Dev. *15*, 859–876.

STAR★METHODS

KEY RESOURCES TABLE

Reagent or resource	Source	Identifier
Antibodies		
Anti-mouse CD45 APC-Cy7	BioLegend	Cat#109824
Anti-mouse CD4 PE610	eBioscience	Cat#61-0042-82
Anti-mouse TCRβ FITC	BioLegend	Cat#109206
Anti-mouse Foxp3 APC	eBioscience	Cat#17-5773-82
Anti-mouse RORγ PE	eBioscience	Cat#12-6988-82
Anti-mouse Helios pacific blue	BioLegend	Cat#137220
Anti-mouse CD44 APC Cy7	BioLegend	Cat#103028
Anti-mouse CD62L PE Cy7	BioLegend	Cat#104418
Anti-mouse Tuj1 (Tubulin β-3)	BioLegend	Cat#802001
Anti-mouse HuC/D	Thermo fisher scientific	Cat#A-21271
Anti-GFP	Abcam	Cat#13970
Anti-mouse EpCAM	BD	Cat#552370
Anti-mouse F4/80	BioLegend	Cat#123101
Donkey anti-rabbit FITC	Jackson Immunoresearch	Cat#711-096-152
Donkey anti-mouse Cy3	Jackson Immunoresearch	Cat#15-165-150
Donkey anti- rat Cy3	Jackson Immunoresearch	Cat#712-166-153
Donkey anti-rabbit Cy2	Jackson Immunoresearch	Cat#711-225-152
Donkey anti-rabbit Cy5	Jackson Immunoresearch	Cat#711-175-152
Goat anti-chicken Alexa488	Thermo fisher scientific	Cat#A-11039
Anti-IL6	BioLegend	Cat# 504505
Anti-OSM	R&D	Cat# AF495-SP
Anti-LIF	R&D	Cat# AF449-SP
Anti-TNFα	BioLegend	Cat# 506309
Anti-IFNγ	BioLegend	Cat# 513206
Anti-IL-1α	BioLegend	Cat# 503206
Anti-CCL-2	BioLegend	Cat# 505905
Anti-CXCL12	R&D	Cat#MAB310
Anti-TNFSF15	BioXCell	Cat#BE0323
functional grade anti-CD3ε	Thermo fisher scientific	Cat#0037-81
Anti-CD3 Biotin	BioLegend	Cat#100304
Anti-TCRβ Biotin	BioLegend	Cat#109204
Chemicals, peptides, recombination proteins		
BD BBL™ Brucella Agar with 5% Sheep Blood	Thermo Fisher scientific	Cat# BD 297848
Collagenase-II	Thermo Fisher scientific	Cat# 17101015
Dispase	Thermo Fisher scientific	Cat# 17105041
Liberase	Roche	Cat# 05401020001
HBSS	Thermo Fisher scientific	Cat# 14185-052
RPMI 1640 medium	Thermo Fisher scientific	Cat# 11875085
FBS	GEMINI	Cat# 100-106
Neurobasal-A medium	Thermo Fisher scientific	Cat# 21103049
B27	Thermo Fisher scientific	Cat# A3582801
Penicillin/streptomycin	Thermo Fisher scientific	Cat# 15140-122

(*Continued on next page*)

Continued

Reagent or resource	Source	Identifier
FGF-b	Peprotech	Cat# 450-33
EGF	Peprotech	Cat# 315-09
NGF	Thermo Fisher scientific	Cat# 50385-MNAC-5
GDNF	Sigma	Cat# SRP3200
Matrigel	Thermo Fisher scientific	Cat# 354234
Accutase	Innovative Cell Technologies	Cat# AT104
Dynabeads® Mouse T-Activator CD3/CD28	Thermo Fisher scientific	Cat# 11453D
Dynabeads Biotin Binder	Thermo Fisher scientific	Cat# 11047
IL-2	Peprotech	Cat# 200-02
TGFβ	Peprotech	Cat#100-21C
Fixation/Permeabilization Concentrate	Thermo Fisher scientific	Cat#00-5123-43
Fixation/Permeabilization Diluent	Thermo Fisher scientific	Cat#00-5223-56
Permeabilization Buffer	Thermo Fisher scientific	Cat#00-8333-56
VIP	Sigma	Cat# V6130
CGRP	Sigma	Cat# C0167
SubstanceP	Sigma	Cat# S6883
Kits		
Mouse IL6 ELISA MAX™ Deluxe	BioLegend	Cat# 431304
Papain Dissociation System	Worthington	Cat# LK003150

RESOURCE AVAILABILITY

Lead Contact

Further information and requests for resources and reagents should be directed to and will be fulfilled by the Lead Contact Prof. Christophe Benoist (cbdm@hms.harvard.edu).

Materials Availability

This study did not generate new unique reagents.

Data and Code Availability

The accession number for the RNA sequencing data reported in this paper on GEO: GSE164577 (RNA profilings of T cells and enteric neuron in T/neuron cocultures, related to Figure 3 FGH), GEO: GSE164576 (RNA profilings of MMP with microbe stimulations, related to Figure 6E) and GEO: GSE164575 (RNA profilings of enteric neurons with microbe stimulations, related to Figure 6 FGH).

EXPERIMENTAL MODEL AND SUBJECT DETAILS

Mice

C57BL/6J (B6), B6.Cg-Foxp3^{tm2Tch}/J (*Foxp3-gfp*), B6.129S4-Vip^{tm1Clw}/J (*Vip*$^{-/-}$), B6.129S2-Il6^{tm1Kopf}/J (Il6$^{-/-}$), B6.SJL-Il6ra$^{tm1.1Drew}$/J (*Il6ra*$^{fl/fl}$), B6.129S1-Stat3^{tm1Xyfu}/J (*Stat3*$^{fl/fl}$), B6.Cg-Tg(Cd4-cre)1Cwi/BfluJ (*CD4-Cre*), B6.Cg-Tac1^{tm1Bbm}/J (*Tac1*$^{-/-}$), B6.Cg-Tg(Nes-cre)^{1Kln}/J (*Nestin-Cre*), B6.Cg-Tg(Syn1-cre)^{617Jxm}/J (*Syn1-Cre*) and B6.CD45,1 mice were obtained from the Jackson Laboratory and bred in the SPF facility at Harvard Medical School (HMS). *Il-6*$^{lox/lox}$ (*Il6*$^{fl/fl}$) (Quintana et al., 2013). B6.129S6-Calca^{tm1}Hku (*Calca*$^{-/-}$), B6.129(Cg)-Ret$^{tm13.1Jmi}$/SjnJ (*Ret-gfp*) and *Calcb*$^{-/-}$ mice (Thompson et al., 2008) were bred in the specific-pathogen-free (SPF) facilities at HMS and BCH. *Ret-gfp* mice were used as hemizygotes. For constitutive genetic deletion, F1 heterozygotes were intercrossed to generate WT and KO littermates. To obtain conditional genetic deletion mice lacking IL6RA and STAT3 in T cells, *Il6ra*$^{fl/fl}$ *and Stat3*$^{fl/fl}$ mice were first crossed with *Cd4-Cre*, then intercrossed to generate WT and *Cd4-Cre Il6ra*$^{fl/fl}$ *and Cd4-Cre Stat3*$^{fl/fl}$ littermates. To obtain mice lacking IL6 in neurons, *Il6*$^{fl/fl}$ mice were first crossed with *Nestin-Cre* and *Syn1-Cre*, then intercrossed to generate WT and neuronal deficient littermates. Only matched littermates were used in control and experimental groups in all experiments. All experimentation was performed following animal protocols approved by the HMS Institutional Animal Use and Care Committee (protocols IS00001257and IS00000054).

METHOD DETAILS

Germ-free mice (GF) and colonization

GF B6 mice (originally obtained from the National Gnotobiotic Rodent Resource Center of the University of North Carolina at Chapel Hill), were bred in the Kasper/Benoist/Mathis shared facility at Harvard Medical School in GF flexible film isolators (Class Biologically Clean). Bacteria (*C.ramosum*, *P.magnus*) were originally obtained from the ATCC or BEI as described (Geva-Zatorsky et al., 2017). Anaerobic bacteria were grown on Brucella 5% SB HEMIN VIT K1 plates (Thermo) under strict anaerobic conditions (80% N_2, 10% H_2, 10% CO_2) at 37°C in an anaerobic chamber, scraped to PBS with 20% glycerol to reach a titer of 109 colonies/mL, and frozen in 100ul aliquots. For colonization, 4-week-old sex-matched GF littermates were divided into control and experimental groups, orally inoculated by gavage with vehicle (PBS plus 20% glycerol) or bacterial aliquots (1 aliquot per mouse), and kept in sterile cages under sterile conditions (sterile food and water).

Enteric neuron cultures

Colons from adult mice (7-12 weeks) were opened lengthwise, and the MMP was dissected completely under a binocular microscope using watchmaker forceps (Zhang and Hu, 2013), cut into pieces of approximately 2 to 5 mm^2 and placed in a 1.5 mL tube containing 50U/mL penicillin and 50ug/mL streptomycin (Thermo Fisher), 0.1mg/mL Liberase TL (Roche) in neutral Hank's Balanced Salt Solution (HBSS, Thermo Fisher) to digest for 0.5 h at 37°C, and then mechanically disrupted by mild shaking. Tissue was then further digested with 0.05% Trypsin -EDTA (Thermo Fisher) solution at 37°C for 10 min. After trituration using a P1000 pipette, single cell suspensions were filtered through 70um filter, cleaned of debris by centrifugation through 1ml fetal bovine serum (110 g for 10min), and captured by selective plating on Matrigel (Thermo Fisher)-coated cell culture dishes in B27 (Thermo Fisher) supplemented Neurobasal-A medium (Thermo Fisher) plus 10 ng/mL fibroblast growth factor-basic (FGF-b, Peprotech), 20ng/mL Epidermal growth factor (EGF, Peprotech), 50U/mL penicillin and 50ug/mL streptomycin (Zhang and Hu, 2013).

Embryonic brain neuron cultures

Papain dissociation (Worthington) were used to prepare neonatal neural cells. Briefly, neonatal mouse brains were minced, digested in Earle's Balanced Salt Solution (EBSS) with papain (20 U/mL, Worthington) for 0.5 h at 37°C and DNase (100U/mL) for 5 min at room temperature. The cell pellets were centrifuged over a 10% BSA at 70 g for 6 min and plated in cell culture dishes in B27 supplemented Neurobasal-A medium plus 50U/mL penicillin and 50ug/mL streptomycin.

DRG neuron cultures

Primary lumber dorsal root ganglia (DRG, segments T7-L6) from adult mice (7–12 weeks) were dissected into Neurobasal-A medium, dissociated in 1 mg/mL collagenase A plus 2.4 U/mL dispase II (Thermo Fisher) in HBSS for 40 min at 37°C. After trituration with glass Pasteur pipettes of decreasing size, DRG cells were centrifuged over a 10% BSA gradient at 260 g for 10 min, plated on Matrigel-coated cell culture dishes in B27 supplemented Neurobasal-A medium supplemented with 50 ng/mL nerve growth factor (NGF, Thermo Fisher), 2 ng/mL glial cell line-derived neurotrophic factor (GDNF, Sigma), 50U/mL penicillin and 50ug/mL streptomycin.

iTreg induction in culture and flow cytometry

Naive CD4+ T splenocytes were sorted as $GFP^-CD4^+CD44^{low}CD62L^{high}$ from *Foxp3-gfp* reporter mice (conjugated mAbs from BioLegend) on a Moflo sorter. Two different protocols were then used: in the first, T cells were activated with anti-CD3/CD28-coated beads (Thermo Fisher) at a concentration of two cells per bead in the presence of 2 U/mL of human rIL-2 and 10 ng/mL rTGF-β (Peprotech) in RPMI with 10% FCS (Chen et al., 2003). In the second, T cells were activated with 1 μg/mL soluble anti-CD3ε (Thermo) presented by T-depleted Mitomycin C (Sigma)-inactivated splenocytes (1:3 ratio) in the presence of 2 U/mL rhIL-2 and 10 ng/mL rTGF-β in RPMI with 10% FCS (Wheaton et al., 2017). To prepare these presenting cells, spleen suspension from congenic *B6.CD45.1* mice were depleted of T cells by incubation with Biotin-conjugated anti-CD3ε (Biolegend) and anti-TCRβ in Dynal buffer (1mg/mL BSA and 2 mM EDTA in PBS) for 20min on ice, washed and incubated with Dynabeads BiotinBinder (150ul per spleen, Thermo) for 30min at 4°C with rotation. T cells were removed using DynaMag magnet (Thermo), and the remaining cells blocked with 0.5mg/mL Mitomycin C at 37°C for 2 h. After 3 days in culture, cells were analyzed by flow cytometry.

T/neuron co-cultures

For T cell and neuron co-cultures, enteric neurons, DRGs or embryonic brain neurons were purified and cultured as above at 5000 cells per well in 96-well plates for 3 days (unless otherwise indicated) and then sorted naive CD4+ T cells were added (100,000 cells per well) for 3 more days using iTreg induction protocols as above. For the co-culture of T cells and neuronal SN, enteric neurons were prepared as above and cultured at a concentration of 10,000 cells per well at 96-well plates for 5 days (unless otherwise indicated), the SN were collected and filtered through 0.22um filter (Millipore), and added to iTreg cultures at 1:4 dilution unless otherwise indicated.

RNaseq profiling

RNA-seq was performed with the standard ImmGen low-input protocol (www.immgen.org). A total of 1,000 cells were sorted directly into 5ul of lysis buffer (TCL Buffer (QIAGEN) with 1% 2-Mercaptoethanol). For cultured neurons, enteric neurons were prepared as

above, cultured for 5 days, detached by Accutase (Innovative) and lyzed in TCL buffer (QIAGEN) with 1% 2-Mercaptoethanol at 1000 cells in 5ul buffer. To profile whole MMP preparations, the fragments were peeled off from the colons, cut into 2cm segments, lyzed and homogenized in 400ul TCL buffer. For primary enteric neurons, the MMP neurons were prepared as above, stained with anti-CD45, Sca1, CD9, and the $CD9^{high}$ population were sorted into TCL buffer at 1000 cells in 5ul buffer. Smart-seq2 libraries were prepared as previously described (Picelli et al., 2014) with slight modifications. Briefly, total RNA was captured and purified on RNAClean XP beads (Beckman Coulter). Polyadenylated mRNA was then selected using an anchored oligo(dT) primer (50 –AAGCAGTGGTAT CAACGCAGAGTACT30VN-30) and converted to cDNA via reverse transcription. First strand cDNA was subjected to limited PCR amplification followed by Tn5 transposon-based fragmentation using the Nextera XT DNA Library Preparation Kit (Illumina). Samples were then PCR amplified for 12 cycles using barcoded primers such that each sample carries a specific combination of eight base Illumina P5 and P7 barcodes for subsequent pooling and sequencing. Paired-end sequencing was performed on an Illumina NextSeq 500 using 2 × 38bp reads with no further trimming. Short reads were then mapped to mm10 genome using hisat2 [version2.0.4 (https://ccb.jhu.edu/software/hisat2/manual.shtml)] with–transcriptome-mapping-only–no-discordant options. Unmapped and low quality scoring (MAPQ < 5) reads were removed using samtools. Moreover, duplicated reads were removed using the Picard MarkDuplicates function. Properly paired reads were selected by samtools view -f 0x02 and counted for each gene using htseqcount (version0.6.1) with -s no option and a GTF file from UCSC mm10 refGene downloaded from UCSC table browser (https://genome.ucsc.edu/cgi-bin/hgTables). Genes with a minimum read count of 5 in all replicates of a population (17,535 genes) were retained. A pseudo count of 1 was added and log2-transformed prior to quantile normalization. Quantile-normalized counts were converted back to a linear scale and means of replicates were calculated for each population.

Flow cytometric analysis

For iTreg in culture, fluorescence from the GFP reporter was measured directly, together with viability detection (stained with 10ug/mL DAPI in PBS for 5min immediately prior to analysis). When required, cells were stained with anti-CD45.1 or anti-CD45, -CD4 and TCRβ for 0.5 h on ice, incubated overnight in Fixation/Permeabilization buffer (Thermo Fisher), and stained with mAbs detecting transcription factors Foxp3, RORγ and Helios (Biolegend) for 40 min at room temperature. Cells were analyzed with a BD LSRII flow cytometer and data were processed with FlowJo software.

Microscopy

For immunostained cryosections, colons from *Foxp3-gfp* mice were fixed with 4% paraformaldehyde (PFA) in PBS for 16 h, equilibrated in 30% sucrose/PBS overnight, embedded in OCT medium (Sakura), and cut into 14um frozen sections using a Leica CM1950 cryostat. Section were washed twice in PBS (20min), blocked with serum (10% in PBS) of the same species as the secondary antibody for 1 h at room temperature, rinsed in staining buffer (1% BSA, 0.3% Tween-20 in PBS), and incubated with primary antibodies against Tuj1 (Biolegend), EpCAM (Becton Dickinson), GFP (Abcam), NOS1 (Abcam) and CGRP (Sigma) for 1 h at room temperature or overnight at 4°C. Tissue sections were then washed 3 times with staining buffer and incubated with secondary antibody (Cy5, Cy3 or FITC-conjugated donkey anti-rabbit/rat/chicken immunoglobulin) for 1 h at room temperature. After washing, sections were mounted with Prolong diamond mounting medium. Images were acquired on a Nikon Ti inverted spinning disk Confocal microscope or a Zeiss LSM700 (63X objective) and processed with ImageJ (Schindelin et al., 2012). All images are either single planar images or maximum intensity projections of z stacks, as detailed in the Figure Legends.

To immunostain cultured cells, cells attached to the glass bottom dishes (Cellvis) were fixed with 4% PFA in PBS overnight on ice, blocked with serum (10% in PBS) of the same species as the secondary antibody for 1 h at room temperature, rinsed in staining buffer, and incubated with primary antibodies against Tuj1 and EpCAM overnight at 4°C. Cells were then washed 3 times with staining buffer, and incubated with Alexa647-conjugated anti-CD45 (Biolegend) and secondary antibody (FITC-conjugated donkey anti-rabbit or anti-rat immunoglobulin) for 1 h at room temperature. After washing, sections were mounted with Prolong mounting medium.

For whole-mount staining, freshly dissected colons were immersed on ice for 20mins in 1uM nicardipine hydrochloride (calcium channel blocker) to maximize smooth muscle relaxation, cut open longitudinally, stretched flat on paper towels, and fixed with 4% PFA overnight on ice. The tissues were bleached by 6% hydrogen peroxide in Methanol in 4°C for 1 h and blocked by Mouse BD Fc Bloc (0.5ug/mL, BD) and 1% donkey serum in PBSGT (0.5%Triton X-100, 0.2% Gelatin in PBS) for 2 days with shaking in 37°C incubator. After incubating with primary antibodies against Tuj1, HuC/D, EpCAM or F4/80 in PBSGT for 3 days and corresponding secondary anti-Ig antibodies for 2 days in the dark at 37°C incubator with shaking, samples were washed and cleared by BABB (1 volume Benzyl Alcohol to 2 volume Benzyl Benzoate) overnight. Tissues were then laid on slides and sealed with nail polish under a coverslip. Z stack images were acquired on an Olympus Fluoview Confocal microscope (0.5um intervals), and IMARIS software used to construct 3D images, Dot module in IMARIS were used to count neurons and Filament module to measure fiber length.

Fluorescence *in situ* hybridization

Probe libraries were designed using the Stellaris FISH Probe Designer Software (Biosearch Technologies). 7-15μm thick sections of fixed colon were sectioned onto poly L-lysine coated coverslips and used for smFISH staining. The colonic sections were hybridized with smFISH probe sets according to a previously published protocol (Itzkovitz et al., 2011). *Foxp3* probe library was labeled with Cy5, *Rorc* library was labeled with Alexa594. Anti-Tuj1 primary antibody was added to the smFISH hybridization buffer and Cy2-conjugated Donkey anti rabbit IgG was added in GLOX buffer for 45 min after DAPI (Sigma-Aldrich, D9542) nuclear staining.

All images were acquired with 100x magnification. Quantification of smFISH was done using ImageJ. 37 cells from 2 mice were quantified. Laplacian of Gaussian filtering was used to enhance mRNA dots.

QUANTIFICATION AND STATISTICAL ANALYSIS

Data were routinely presented as mean ± SD. Unless stated otherwise, significance was assessed by Student's t test using GraphPad Prism 8.0.